MAGNETIC RESONANCE IN CHEMISTRY
Magn. Reson. Chem. 2007; **45**: 296–316
Published online in Wiley InterScience
(www.interscience.wiley.com) DOI: 10.1002/mrc.1966

MRC

Broadband proton-decoupled proton spectra†

Andrew J. Pell,[1] Richard A. E. Edden[2] and James Keeler[1]*

[1] Department of Chemistry, University of Cambridge, Lensfield Road, Cambridge CB2 1EW, UK
[2] Russell H. Morgan Department of Radiology and Radiological Science, Johns Hopkins University School of Medicine, 600 North Wolfe Street, Baltimore, MD 21287, USA

Received 23 October 2006; Revised 18 December 2006; Accepted 1 January 2007

We present a new method for recording broadband proton-decoupled proton spectra with absorption mode lineshapes and substantially correct integrals; in both these respects, the new method has significant advantages over conventional *J*-spectroscopy. In our approach, the decoupled spectrum is simply obtained from the 45° projection of the diagonal-peak multiplets of an anti *z*-COSY spectrum. This method is straightforward to apply, and does not require any unusual data processing. However, there is a significant reduction in sensitivity when compared to a conventional proton spectrum. The method is demonstrated for typical medium-sized molecules, and it is also shown how such a decoupled spectrum can be used to advantage in measurements of diffusion constants (DOSY), the measurement of relaxation parameters, and the analysis of complex mixtures. Copyright © 2007 John Wiley & Sons, Ltd.

KEYWORDS: NMR; broadband decoupling; Z-COSY; diffusion; DOSY

INTRODUCTION

In this paper, we describe a new method for generating proton-decoupled proton spectra – that is, proton spectra that contain a single line for each chemically distinct site, not split by the effects of scalar couplings. Our method is distinguished by the fact that the decoupled spectra have absorption mode lineshapes and retain the correct integrals, i.e. the integral is proportional to the number of equivalent protons. Furthermore, the method is experimentally straightforward and does not require any unusual data processing. We therefore believe that it offers a number of significant advantages over the existing approaches for obtaining proton-decoupled proton spectra.

The simplification resulting from the elimination of multiplet structures may be advantageous in a number of areas, such as in the analysis of complex mixtures, which arise from studies of metabolism. Any quantitative measurements, such as the measurement of relaxation rate constants and diffusion constants, will also benefit from the reduction in overlap, which is a feature of proton-decoupled proton spectra.

The new method utilizes a two-dimensional anti *z*-COSY spectrum.[1] It will be shown that a 45° projection of the diagonal-peak multiplets of such a spectrum gives the required absorption mode decoupled spectrum. As the pulse sequence for *z*-COSY includes two small flip angle pulses, there is a loss in sensitivity when compared to a simple proton spectrum. A further problem is that the presence of strong coupling gives rise to unwanted peaks in the projection, in a way analogous to those found in two-dimensional *J*-spectra.[2–4]

*Correspondence to: James Keeler, Department of Chemistry, University of Cambridge, Lensfield Road, Cambridge CB2 1EW, UK. E-mail: jhk10@cam.ac.uk
†Presented at the 47th ENC, Asilomar, California, USA, 2006.

OUTLINE OF THE METHOD

The pulse sequences for the *z*-COSY and anti *z*-COSY experiments are shown in Fig. 1.[1] Both experiments give spectra that are closely related to the simple COSY spectrum,[5,6] with cross-peak multiplets indicating the presence of scalar couplings, and a set of diagonal-peak multiplets arranged along the 45° diagonal. In COSY, the mixing period is a simple 90° pulse, but in *z*-COSY the mixing period is the element $\beta - t_z - \beta$, where β is a small flip angle pulse, and where only population terms are retained during the short delay t_z. The use of this mixing period gives rise to *reduced* cross- and diagonal-peak multiplets. In such multiplets, the only peaks that are seen are those in which the spin states of any passive spins remain the *same* during t_1 and t_2. This key idea is illustrated in Fig. 2, which shows a typical diagonal- and cross-peak multiplet for a three-spin system. Each line has been labelled with the spin states of the passive spins, and we note that only those with the same spin states in t_1/ω_1 and t_2/ω_2 are present. For the diagonal-peak multiplet, this means that all the peaks lie along the 45° diagonal.

In the case of anti *z*-COSY, the mixing sequence is $(\beta + \pi) - t_z - \beta$. The addition of the 180° pulse at the beginning means that all the spin states are flipped, so this time the only peaks that appear in the multiplet are those with *opposite* spin states in t_1/ω_1 and t_2/ω_2. As a result, as shown in Fig. 2 (c), the peaks in the diagonal-peak multiplet lie on a line which is perpendicular to the main diagonal. If we project this diagonal-peak multiplet onto the main diagonal, we obtain a single peak at the chemical shift; this is the basis of our method.

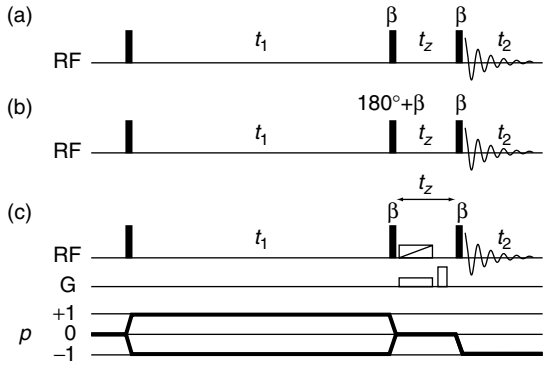

Figure 1. Pulse sequences for: (a) *z*-COSY, (b) anti *z*-COSY, and (c) anti *z*-COSY with zero-quantum suppression. All three sequences follow the same coherence transfer pathway (CTP), which is shown at the bottom. The mixing period for *z*-COSY comprises a *z*-filter in which both pulses have flip angle β, where β is small. The two mixing pulses for anti *z*-COSY have flip angles of $180^\circ + \beta$ and β. The anti *z*-COSY sequence shown in (c) incorporates the swept-frequency 180° pulse (indicated by the open rectangle with the diagonal stroke) and gradient combination for the suppression of zero-quantum coherence present during t_z. The second gradient is a homospoil that is used to dephase all coherences with nonzero order. Note that in this experiment, both mixing pulses have flip angle β. All pulses are of phase *x* and, unless otherwise indicated, the filled rectangles represent 90° pulses.

The beauty of this approach is that the diagonal peaks of the anti *z*-COSY spectrum are all in absorption mode, so the projection is also in the absorption mode. Furthermore, as the number of individual peaks in the diagonal-peak multiplet is the same as in the regular multiplet, the integral of the peak in the projection is the same as for the corresponding multiplet, apart from a simple scaling factor due to the mixing period, which is common to all multiplets. As a result, the projection will give reliable integrals – we can describe the projection as being quantitative.

In the past, *z*-COSY spectra have been bedeviled by phase distortions resulting from the presence of zero-quantum coherence present during t_z. However, it has recently been shown that these unwanted coherences can be suppressed effectively and conveniently using the combination of a swept-frequency 180° pulse and a modest gradient.[7,8] Such a combination dephases the zero-quantum coherence in a way analogous to the dephasing of other coherences by gradients. Figure 1 (c) shows the pulse sequence for anti *z*-COSY which incorporates this zero-quantum dephasing method. Note that on account of the swept 180° pulse, the additional 180° pulse used in the mixing sequence of (b) is not needed in sequence (c).

There are a number of issues that need to be addressed if the projection method is to be a practical approach. The first is that, as the projection is at 45°, the linewidth in the projection is an average of the linewidths in the ω_1 and ω_2 dimensions. It is therefore essential to acquire the spectra with high resolution in the ω_1 dimension, implying that t_1 must extend to quite long times. For a typical ω_1 spectral width, this need for a large $t_1^{\max}$ means that many increments of t_1 must be recorded. In cases where the sensitivity is high, this may lead to an unnecessarily long minimum experiment time.

It would therefore be advantageous to reduce the number of t_1 increments by reducing the ω_1 spectral width. Inevitably, this will lead to a folding in the ω_1 dimension, but it will be shown that such folding does not cause significant difficulties in obtaining the required projection.

The second point that needs to be addressed is the presence of cross-peak multiplets, which are inevitably generated by the mixing period. These multiplets must not be included in the projection, as doing so will lead to unwanted anti-phase multiplets in the projection. If such cross-peak multiplets lie well away from the main diagonal, then it is easy to exclude them from the projection. It will be

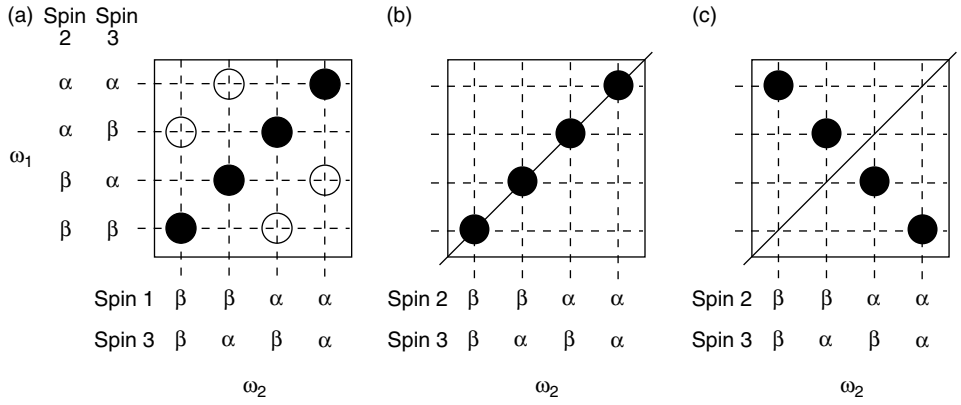

Figure 2. Schematic diagonal- and cross-peak multiplets expected in the *z*-COSY and anti *z*-COSY spectra of a three-spin system. Shown in (a) is the cross-peak multiplet between spins one and two in the *z*-COSY spectrum; the spin states of the passive spins are indicated in each dimension. The diagonal-peak multiplet of spin one in the *z*-COSY spectrum is shown in (b). The only peaks that are present are those in which the spin states of the passive spins are the same in both dimensions. As a result, the peaks lie along the 45° diagonal. In contrast, the only peaks that are observed in the diagonal-peak multiplet of the anti *z*-COSY spectrum, which is shown in (c), are those in which the passive spins have the opposite spin state in each dimension; the peaks therefore lie along a line that is perpendicular to the diagonal. It is assumed that $J_{12} > J_{13} = J_{23}$. Filled circles represent peaks of positive intensity, and unfilled circles represent peaks of negative intensity.

DOI: 10.1002/mrc

shown that if these peaks have been folded in ω_1, as a result of using a reduced spectral width in that dimension, they acquire symmetry properties, which means that they can be eliminated by a simple data processing method. However, if the cross-peak multiplets lie close to the diagonal, and are not folded, it may be not possible to exclude them from the projection. Of course, cross peaks that lie close to the diagonal are ones in which the difference of the offsets of the two spins is becoming comparable to the scalar coupling, which is exactly the condition for strong coupling. So, the contribution of these cross peaks to the projection is analogous to the presence of 'strong coupling artifacts' in two-dimensional *J*-spectra.[2–4]

THEORETICAL ANALYSIS

In this section, we will analyze the various stages used to generate the required projection. It is sufficient to use a three-spin system as the example, as this demonstrates all the relevant properties. Since we are interested in multiplet structures it is convenient to use single-element basis operators as they have a one-to-one correspondence with the lines in the spectrum.

Anti *z*-COSY

The initial state is chosen to be equilibrium magnetization on spin one. The 90° pulse generates in-phase magnetization along the $-y$-axis, $-\hat{I}_{1y}$, which can be expressed in single-element operators as

$$\frac{1}{2}\mathrm{i}(\hat{I}_{1+}\hat{I}_{2\alpha}\hat{I}_{3\alpha} + \hat{I}_{1+}\hat{I}_{2\alpha}\hat{I}_{3\beta} + \hat{I}_{1+}\hat{I}_{2\beta}\hat{I}_{3\alpha} + \hat{I}_{1+}\hat{I}_{2\beta}\hat{I}_{3\beta})$$
$$-\frac{1}{2}\mathrm{i}(\hat{I}_{1-}\hat{I}_{2\alpha}\hat{I}_{3\alpha} + \hat{I}_{1-}\hat{I}_{2\alpha}\hat{I}_{3\beta} + \hat{I}_{1-}\hat{I}_{2\beta}\hat{I}_{3\alpha} + \hat{I}_{1-}\hat{I}_{2\beta}\hat{I}_{3\beta})$$

The terms containing $\hat{I}_{1+}$ will produce the echo (N-type) spectrum, while those containing $\hat{I}_{1-}$ will produce the anti-echo (P-type) spectrum.

Each of these terms evolves at its characteristic frequency during t_1 to give:

$$\begin{aligned}
&\frac{1}{2}\mathrm{i}\xi\hat{I}_{1\pm}\hat{I}_{2\alpha}\hat{I}_{3\alpha} && \frac{1}{2}\mathrm{i}\xi\hat{I}_{1\pm}\hat{I}_{2\alpha}\hat{I}_{3\alpha}\exp[\mp\mathrm{i}(\Omega_1 + \pi J_{12} + \pi J_{13})t_1]\\
&\frac{1}{2}\mathrm{i}\xi\hat{I}_{1\pm}\hat{I}_{2\alpha}\hat{I}_{3\beta} && \frac{1}{2}\mathrm{i}\xi\hat{I}_{1\pm}\hat{I}_{2\alpha}\hat{I}_{3\beta}\exp[\mp\mathrm{i}(\Omega_1 + \pi J_{12} - \pi J_{13})t_1]\\
&\qquad\xrightarrow{\hat{H}_{\mathrm{free}}t_1} &&\\
&\frac{1}{2}\mathrm{i}\xi\hat{I}_{1\pm}\hat{I}_{2\beta}\hat{I}_{3\alpha} && \frac{1}{2}\mathrm{i}\xi\hat{I}_{1\pm}\hat{I}_{2\beta}\hat{I}_{3\alpha}\exp[\mp\mathrm{i}(\Omega_1 - \pi J_{12} + \pi J_{13})t_1]\\
&\frac{1}{2}\mathrm{i}\xi\hat{I}_{1\pm}\hat{I}_{2\beta}\hat{I}_{3\beta} && \frac{1}{2}\mathrm{i}\xi\hat{I}_{1\pm}\hat{I}_{2\beta}\hat{I}_{3\beta}\exp[\mp\mathrm{i}(\Omega_1 - \pi J_{12} - \pi J_{13})t_1]
\end{aligned}$$

where ξ is equal to $+1$ for the echo and -1 for the anti-echo, and $\hat{\mathcal{H}}_{\mathrm{free}}$ is the free-precession Hamiltonian.

The first mixing pulse can be treated as two separate pulses of flip angles π and β that act consecutively. The 180° pulse changes the sign of the coherence order and converts $\hat{I}_{i\alpha}$ to $\hat{I}_{i\beta}$, and vice versa. For example, the operators $\frac{1}{2}\mathrm{i}\hat{I}_{1\pm}\hat{I}_{2\alpha}\hat{I}_{3\alpha}$ are transformed as follows:

$$\frac{1}{2}\mathrm{i}\xi\hat{I}_{1\pm}\hat{I}_{2\alpha}\hat{I}_{3\alpha}\exp[\mp\mathrm{i}(\Omega_1 + \pi J_{12} + \pi J_{13})t_1] \xrightarrow{\pi\hat{F}_x}$$
$$\frac{1}{2}\mathrm{i}\xi\hat{I}_{1\mp}\hat{I}_{2\beta}\hat{I}_{3\beta}\exp[\mp\mathrm{i}(\Omega_1 + \pi J_{12} + \pi J_{13})t_1]$$

where $\hat{F}_x = \hat{I}_{1x} + \hat{I}_{2x} + \hat{I}_{3x}$.

The rotation of single-element operators by radiofrequency pulses is described by the following equations:

$$\hat{I}_{n\pm} \xrightarrow{\beta\hat{I}_{nx}} \hat{I}_{n\pm}c^2 + \hat{I}_{n\mp}s^2 \pm \frac{1}{2}\mathrm{i}(\hat{I}_{n\alpha} - \hat{I}_{n\beta})S \quad (1)$$

$$\hat{I}_{n\alpha} \xrightarrow{\beta\hat{I}_{nx}} \hat{I}_{n\alpha}c^2 + \hat{I}_{n\beta}s^2 + \frac{1}{2}\mathrm{i}(\hat{I}_{n+} - \hat{I}_{n-})S \quad (2)$$

$$\hat{I}_{n\beta} \xrightarrow{\beta\hat{I}_{nx}} \hat{I}_{n\beta}c^2 + \hat{I}_{n\alpha}s^2 - \frac{1}{2}\mathrm{i}(\hat{I}_{n+} - \hat{I}_{n-})S \quad (3)$$

where $c = \cos\frac{\beta}{2}$, $s = \sin\frac{\beta}{2}$, and $S = \sin\beta$. If β is small, then s^2, which is of the order $\mathcal{O}(\beta^2)$, tends to zero, and Eqns 1, 2, and 3 can be approximated as:

$$\hat{I}_{n\pm} \xrightarrow{\beta\hat{I}_{nx}} \hat{I}_{n\pm}c^2 \pm \frac{1}{2}\mathrm{i}(\hat{I}_{n\alpha} - \hat{I}_{n\beta})S$$

$$\hat{I}_{n\alpha} \xrightarrow{\beta\hat{I}_{nx}} \hat{I}_{n\alpha}c^2 + \frac{1}{2}\mathrm{i}(\hat{I}_{n+} - \hat{I}_{n-})S$$

$$\hat{I}_{n\beta} \xrightarrow{\beta\hat{I}_{nx}} \hat{I}_{n\beta}c^2 - \frac{1}{2}\mathrm{i}(\hat{I}_{n+} - \hat{I}_{n-})S$$

Therefore, after the first β pulse a typical term such as $\frac{1}{2}\mathrm{i}\xi\hat{I}_{1\mp}\hat{I}_{2\beta}\hat{I}_{3\beta}$ becomes:

$$\frac{1}{2}\mathrm{i}\xi\left(\hat{I}_{1\mp}c^2 \mp \frac{1}{2}\mathrm{i}(\hat{I}_{1\alpha} - \hat{I}_{1\beta})S\right)\left(\hat{I}_{2\beta}c^2 - \frac{1}{2}\mathrm{i}(\hat{I}_{2+} - \hat{I}_{2-})S\right)$$
$$\times\left(\hat{I}_{3\beta}c^2 - \frac{1}{2}\mathrm{i}(\hat{I}_{3+} - \hat{I}_{3-})S\right)$$

Of the many terms here, only those representing populations are retained in the anti *z*-COSY sequence; these are

$$\frac{1}{4}Sc^4(\hat{I}_{1\alpha}\hat{I}_{2\beta}\hat{I}_{3\beta} - \hat{I}_{1\beta}\hat{I}_{2\beta}\hat{I}_{3\beta})$$

There are some other population terms that are of higher order in $\sin\beta$; these can be neglected as β is small.

The final β pulse produces the following observable terms, which all carry a t_1 phase factor of $\exp[\mp\mathrm{i}(\Omega_1 + \pi J_{12} + \pi J_{13})t_1]$:

diagonal peak on spin one:

$$-\frac{1}{4}\mathrm{i}S^2c^8\hat{I}_{1-}\hat{I}_{2\beta}\hat{I}_{3\beta}$$

cross peaks between spins one and two:

$$\frac{1}{8}\mathrm{i}S^2c^8\hat{I}_{1\alpha}\hat{I}_{2-}\hat{I}_{3\beta} - \frac{1}{8}\mathrm{i}S^2c^8\hat{I}_{1\beta}\hat{I}_{2-}\hat{I}_{3\beta}$$

cross peaks between spins one and three:

$$\frac{1}{8}\mathrm{i}S^2c^8\hat{I}_{1\alpha}\hat{I}_{2\beta}\hat{I}_{3-} - \frac{1}{8}\mathrm{i}S^2c^8\hat{I}_{1\beta}\hat{I}_{2\beta}\hat{I}_{3-}$$

The calculation can be repeated for the other terms to give the full multiplet structures of the spin-one diagonal peak, and the associated cross-peaks.

DOI: 10.1002/mrc

Every peak in the N-type spectrum is matched by a peak in the P-type spectrum with the same intensity, but with the opposite sense of modulation during t_1. Therefore, the two experiments can be combined to give a spectrum which has frequency discrimination in ω_1 and absorption mode lineshapes. Furthermore, both the cross peaks and diagonal peaks have the same phase in both frequency dimensions, and so it is possible to phase the spectrum so that both the cross peaks and the diagonal peaks have the double-absorption lineshape.

Diagonal-peak multiplet

We have seen from our analysis that, for the diagonal-peak terms, each operator product present prior to t_1 gives only one operator during t_2. Therefore, the diagonal-peak multiplet will have four lines of equal intensities, at unique frequencies in each dimension. The position of each peak in ω_2 is the same as that in ω_1, except that *all* the coupling constant terms have *opposite* sign. This is because the passive spins have the opposite spin polarization during t_2 to the one they have during t_1, since there a high probability that the first mixing pulse (flip angle $\beta + 180^\circ$) will change the spin states of the passive spins, and the second mixing pulse (flip angle β) leaves their polarization unaffected. These peaks all lie on the counter-diagonal, giving the multiplet structure shown in Fig. 2 (c).

This multiplet has a complete separation of the offset and the coupling: the frequency dimension that is parallel to the diagonal contains only the offset information, and the counter-diagonal dimension contains only coupling information. Therefore, the projection of the multiplet onto the diagonal is a decoupled spectrum.

A more detailed calculation, which does not discard any population terms, gives the set of intensities for the diagonal peaks shown in Table 1. There are three types of peak, which are illustrated in Fig. 3.

Type 1 peaks lie on the counter-diagonal, and are the ones we require. The peaks of type 3 lie on the diagonal and are due to magnetization terms in which the passive spins do not experience a net change of polarization during the mixing period. Their intensity varies as $\sin^2\beta\cos^4(\beta/2)\sin^4(\beta/2)$, which is negligible for small β, and so they do not need to be considered further. The peaks of type 2 are more intense, as the leading term in the expression for their intensity varies as $\sin^2\beta\cos^6(\beta/2)\sin^2(\beta/2)$. Considering only the leading terms, the ratio of the intensity of these unwanted peaks to

Table 1. The positions and intensities of the three types of peak in the diagonal-peak multiplet of spin one from the anti z-COSY spectrum of a three-spin system. $S = \sin\beta$ and $c = \cos(\beta/2)$

Type	Description	Intensity
1	Counter-diagonal peak	$-\frac{1}{4}iS^2(c^8 + 2c^4s^4 + s^8)$
2	Off-diagonal peak	$-\frac{1}{2}iS^2(c^6s^2 + c^2s^6)$
3	On-diagonal peak	$-iS^2c^4s^4$

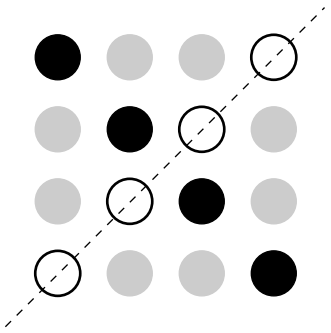

Figure 3. Schematic of the spin-one diagonal-peak multiplet of a three-spin system showing the three types of peaks. The black circles represent the counter-diagonal peaks (type 1), the grey circles represent the off-diagonal peaks (type 2), and the on-diagonal peaks (type 3) are represented by the unfilled circles. The position of the main diagonal is given by the dashed line.

the intensity of the wanted counter-diagonal peaks (type 1) is

$$\frac{\text{type 2}}{\text{type 1}} = \frac{2\sin^2(\beta/2)}{\cos^2(\beta/2)} = 2\tan^2(\beta/2)$$

For a flip angle of $\beta = 20^\circ$, the off-diagonal peaks have a relative intensity of 0.062, or 16 : 1. If $\beta = 10^\circ$, the relative intensity is 0.015, or 67 : 1. The peaks that do not lie on the counter-diagonal will give rise to unwanted peaks in the projection. These unwanted components must be minimized, which is done by reducing the value of β. However, the intensity of the wanted peaks, which includes a factor of $\sin^2\beta$, will also be reduced. Therefore, a compromise must be made in which β is small enough to suppress the unwanted diagonal peaks, but large enough to retain sufficient intensity in the counter-diagonal peaks. Typically, we use a flip angle between 10° and 20°.

This analysis assumes that each population term that is present immediately after the first β pulse will be unchanged at the end of t_z. However, any longitudinal relaxation that occurs during this delay may cause the polarization of the spins to change. This leads to transformations such as

$$\hat{I}_{1\alpha}\hat{I}_{2\beta}\hat{I}_{3\beta} \longrightarrow \hat{I}_{1\alpha}\hat{I}_{2\beta}\hat{I}_{3\alpha}$$

Spin three has therefore not experienced a net change in its spin state during the mixing period, and so these relaxation processes lead to an increase in the intensity of the undesirable peaks (here type 2). This effect can be minimized by keeping the delay t_z as short as possible. In practice, this means that t_z is made just long enough for the required zero-quantum suppression.

PROJECTING THE SPECTRUM

As has been explained, the required decoupled spectrum is the projection of the anti z-COSY spectrum onto the 45° diagonal. In this section we consider the details of how this projection is calculated and what its properties are. There

DOI: 10.1002/mrc

are two ways in which we could imagine calculating this projection. The first is to rotate the two-dimensional spectrum such that the 45° diagonal is horizontal. Projecting onto this axis gives the required spectrum. The second approach is to shear the spectrum so as to align the multiplets in the correct way, and then compute the projection.

In practice, the two methods are equivalent; however, it is conceptually easier to start with the rotation, but computationally simpler to use the shear. We will therefore describe both methods.

The projection of a two-dimensional spectrum $\tilde{S}(\omega_1, \omega_2)$ onto an axis u_2 is calculated by integrating over the perpendicular dimension u_1. According to the projection cross-section theorem,[9] this is equivalent to extracting and Fourier transforming the relevant cross-section from the time-domain, as shown in Fig. 4(a). In the case we are interested in, u_2 is the axis that passes through the origin and is tilted at an angle ϕ to the ω_1 axis, as is illustrated in Fig. 4(b).

Mathematically, the projection of a two-dimensional spectrum onto u_2 is most easily calculated by first rotating the spectrum through $\pi/2 - \phi$, so that u_2 coincides with the ω_2 axis. This rotation is described by the following frequency-coordinate transformation:

$$u_1 = \omega_1 \sin\phi - \omega_2 \cos\phi \tag{4}$$

$$u_2 = \omega_1 \cos\phi + \omega_2 \sin\phi \tag{5}$$

The projection onto the u_2 axis is then given by:

$$P(u_2) = \int_{-\infty}^{\infty} \tilde{S}(u_1 \sin\phi + u_2 \cos\phi, -u_1 \cos\phi + u_2 \sin\phi) \mathrm{d}u_1$$

A projection onto the main diagonal is achieved with $\phi = \pi/4$:

$$u_1 = \frac{1}{\sqrt{2}}\omega_1 - \frac{1}{\sqrt{2}}\omega_2 \tag{6}$$

$$u_2 = \frac{1}{\sqrt{2}}\omega_1 + \frac{1}{\sqrt{2}}\omega_2 \tag{7}$$

Rather than rotating the spectrum, in practice it is usually easier to use the standard software to shear the spectrum, so that the diagonal and counter-diagonal coincide with the ω_2 and ω_1 axes; we then project onto ω_2. A shear operation applied parallel to the ω_1 axis is illustrated in Fig. 5 for the case of a unit square data matrix.

Each point is translated in the ω_1-direction by an amount $\Delta\omega_1$ that is proportional to its ω_2-coordinate. This can be expressed mathematically as

$$\Delta\omega_1 = \alpha\omega_2$$

where the constant of proportionality α is referred to as the *shear rate*. The ω_1 axis, which is invariant under this transformation, is called the shear axis. It is also possible to define a *shear angle* θ as

$$\tan\theta = \alpha$$

which is the angle through which a line that is perpendicular to the shear axis is tilted.

The shear transforms the square frequency space into a rhombus. One of the consequences of this is that there are two regions of the spectrum (shaded grey in Fig. 5 (b)) that are shifted outside of the original square window. It is usual to translate (wrap) these regions back inside the

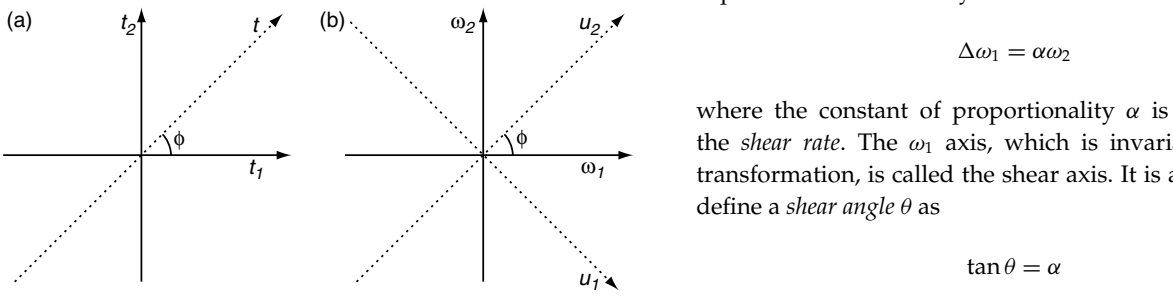

Figure 4. Illustration of the projection cross-section theorem. The time domain is shown in (a), and the frequency domain in (b). According to the theorem, the Fourier transform of a cross-section that passes through the origin and is inclined at an angle ϕ to the t_1 axis is the same as the frequency-domain projection onto the axis u_2, which is inclined at the same angle to the ω_1 axis.

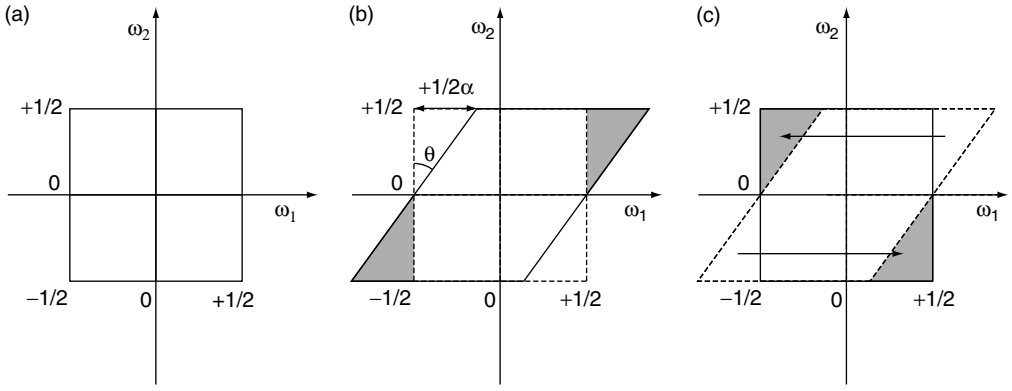

Figure 5. Illustration of a shear on a unit square. The unit square shown in (a) is sheared parallel to ω_1 to give the rhombus in (b). The grey regions have been shifted outside the boundary of the square. They are translated back inside, as indicated by the arrows, to give the square data matrix shown in (c).

DOI: 10.1002/mrc

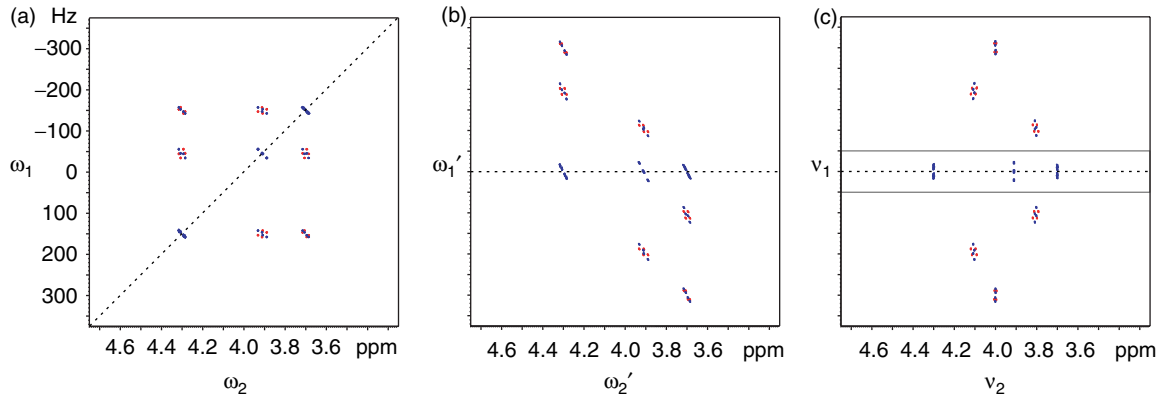

Figure 6. The effect of the required two shears on a simulated anti *z*-COSY spectrum of a three-spin system. The main diagonal is indicated by a dashed line. Positive contours are colored blue, and negative contours are red. See text for details of the shear operations relating (b) to (a), and (c) to (b).

original window, as shown in Fig. 5 (c). As a result, data points lying on a line parallel to the shear axis undergo a cyclic rearrangement.

In order to transform the anti *z*-COSY spectrum in such a way that the projection onto one axis gives the required proton-decoupled spectrum, two shears are needed. The process is shown for a simulated spectrum of a three-spin system in Fig. 6.

The original spectrum (a) is first sheared parallel to ω_1, with a shear rate of $\alpha_1 = -1$; this gives spectrum (b). Such a shear transforms the frequency space (ω_1, ω_2) into a new coordinate system (ω_1', ω_2') as follows:

$$\begin{aligned}\omega_1' &= \omega_1 + \alpha_1\omega_2 \\ &= \omega_1 - \omega_2 \\ \omega_2' &= \omega_2\end{aligned}$$

In such a spectrum, what was the diagonal is now parallel to ω_2', but the diagonal-peak multiplets are still tilted with respect to ω_1'. The second shear is parallel to ω_2', with a shear rate of $\alpha_2 = +\frac{1}{2}$, which gives a spectrum with the coordinate system (v_1, v_2):

$$\begin{aligned}v_1 &= \omega_1' \\ &= \omega_1 - \omega_2 \qquad (8) \\ v_2 &= \omega_2' + \alpha_2\omega_1' \\ &= \frac{1}{2}\omega_1 + \frac{1}{2}\omega_2 \qquad (9)\end{aligned}$$

This gives the spectrum shown in (c), in which the multiplets are parallel to v_1, as required.

On comparing Eqns (6) and (7) with Eqns (8) and (9), it is seen that

$$v_1 = \sqrt{2}u_1 \qquad (10)$$

$$v_2 = \frac{u_2}{\sqrt{2}} \qquad (11)$$

Therefore, the two shears are equivalent to a 45° rotation of the spectrum followed by a scaling operation, parallel to each of the two rotated axes, as indicated by Eqns (10) and (11). The scaling is entirely trivial as both the linewidth and the frequency axes are scaled in the same way. The resolution is therefore the same.

The sheared spectrum has a complete separation of the offset and coupling information. The projection of the diagonal peaks onto the v_2 axis is a one-dimensional spectrum in which there is just one line per chemical environment. This projection is calculated by selecting the region of the spectrum which contains only the diagonal-peak multiplets, as shown by the grey box in Fig. 6 (c), and summing over the data points in the v_1 dimension. The projected region is shown in Fig. 7 along with the decoupled spectrum.

In addition, a cross-section that is taken parallel to v_1 at the position of the offset in v_2 gives the structure of the associated multiplet. These cross-sections at the offsets of the three spins are shown in Fig. 8(a)–(c).

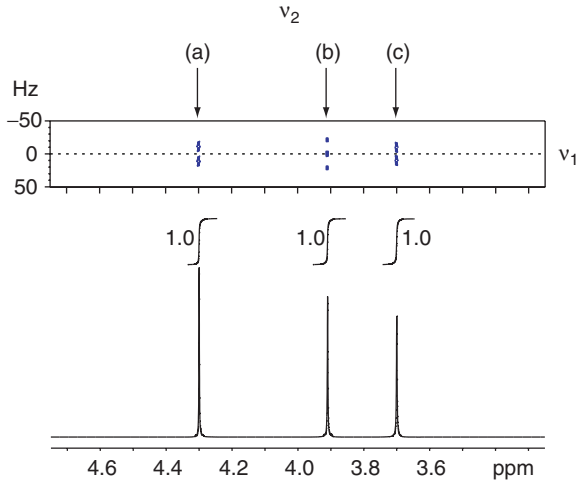

Figure 7. The region of the spectrum of Fig. 6 (c) that is projected. The projection itself is shown below, with the integrals of the three peaks. The values of T_2 that were used are in the ratio 2 : 1.33 : 1. The three arrows labelled (a) – (c) indicate the positions at which the vertical cross-sections shown in Fig. 8 are taken.

DOI: 10.1002/mrc

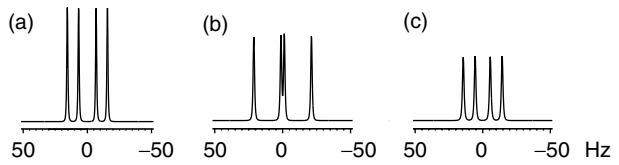

Figure 8. The cross-sections of the doubly sheared anti *z*-COSY spectrum of the three-spin system, taken at positions (a), (b), and (c) as shown in Fig. 7. As the cross-sections are taken parallel to v_1, they give the structure of each multiplet.

LINESHAPES AND SIGNAL-TO-NOISE RATIO

Linewidths

In this section, we will show that a peak in the projection has an absorption mode lineshape, with a linewidth that is the average of the linewidths in the ω_1 and ω_2 dimensions.

A two-dimensional double-absorption Lorentzian that is centered on $(\omega_1, \omega_2) = (\Omega_1, \Omega_2)$ is represented by the following function

$$A(\omega_1, \omega_2) = \frac{R_1 R_2}{(R_1^2 + (\omega_1 - \Omega_1)^2)(R_2^2 + (\omega_2 - \Omega_2)^2)}$$

where $R_1 = 1/T_2^{(1)}$ and $R_2 = 1/T_2^{(2)}$; $T_2^{(1)}$ and $T_2^{(2)}$ are the transverse relaxation time constants during t_1 and t_2 respectively. The linewidth, conventionally taken to be the full width at half-maximum (FWHM) in the ω_i dimension is $2R_i$ rad s^{-1}.

After the rotation described by Eqns 4 and 5, the lineshape function takes the form

$$\begin{aligned} A(u_1, u_2) = {} & R_1 R_2 (R_1^2 + (u_1 \sin\phi + u_2 \cos\phi - \Omega_1)^2)^{-1} \\ & \times (R_2^2 + (-u_1 \cos\phi + u_2 \sin\phi - \Omega_2)^2)^{-1} \end{aligned}$$

The lineshape in the projection is given by integrating this lineshape function over u_1. The required projection can, however, be calculated more easily by using the projection cross-section theorem,[9] and is

$$P(u_2) = \frac{\pi R'}{R'^2 + (u_2 - \Omega')^2}$$

where $R' = R_1|\cos\phi| + R_2|\sin\phi|$, and $\Omega' = \Omega_1 \cos\phi + \Omega_2 \sin\phi$. The peak therefore has a linewidth of $2R'$ rad s^{-1}, which is a weighted average of the ω_1 and ω_2 linewidths, and appears at a position that is a weighted average of the offsets in the two dimensions. If $\phi = \pi/4$, the linewidth and position of the peak in the projection become:

$$2R' = \frac{2}{\sqrt{2}}(R_1 + R_2)$$

$$\Omega' = \frac{1}{\sqrt{2}}(\Omega_1 + \Omega_2)$$

In practice, instead of rotating the spectrum we shear it; this process results in a spectrum with the following double-absorption Lorentzian lineshape:

$$\begin{aligned} A(v_1, v_2) = {} & R_1 R_2 \left(R_1^2 + \left(\frac{1}{2} v_1 + v_2 - \Omega_1 \right)^2 \right)^{-1} \\ & \times \left(R_2^2 + \left(-\frac{1}{2} v_1 + v_2 - \Omega_2 \right)^2 \right)^{-1} \end{aligned}$$

Integrating this with respect to v_1 (i.e. projecting onto v_2) gives the following lineshape:

$$P(v_2) = \frac{\pi R_\mathrm{p}}{R_\mathrm{p}^2 + (v_2 - \Omega_\mathrm{p})^2}$$

where

$$R_\mathrm{p} = \frac{1}{2}(R_1 + R_2) \tag{12}$$

$$\Omega_\mathrm{p} = \frac{1}{2}(\Omega_1 + \Omega_2) \tag{13}$$

This offset and linewidth are the same as the corresponding values in the projection of the spectrum that has been rotated by 45°, except for a scaling factor of $1/\sqrt{2}$. As we noted above, the frequency axes are scaled in the same way, so the resolution is the same.

In the presence of significant inhomogeneous broadening, the lineshape becomes elongated along the principal diagonal.[10] However, the linewidth in the projection of the sheared spectrum is still the average of the linewidths in the two dimensions, although the lineshape will reflect the exact form of the inhomogeneity.

The data may be processed with weighting functions in either or both dimensions, although, if the correct integrals are to be retained, these weighting functions must always decay from the value at $t_1 = 0$ or $t_2 = 0$. Given that sampling may be limited in t_1, it may be necessary to apodize the data in this dimension in order to avoid truncation artifacts. However, the resulting extra line broadening in the ω_1 dimension is undesirable as it is transferred to the projection. In this paper all of the experimental spectra have been processed without weighting functions unless otherwise indicated.

Sensitivity

We will now compare the sensitivities of the proton-decoupled spectrum and a conventional one-dimensional spectrum. This comparison is done by calculating the signal-to-noise ratio (SNR) of a singlet in each spectrum. Without loss of generality, we assume that the singlet is on resonance.

In a conventional proton spectrum that is acquired with a single scan, the height of the peak is S, and the rms noise amplitude is σ, giving an SNR of S/σ.

The anti *z*-COSY spectrum is recorded with N_1 t_1-increments. It is assumed that the linewidths are the same in both ω_1 and ω_2, so that the shearing does not affect the SNR in the projection. We will therefore simply calculate the signal-to-noise ratio of the singlet in the ω_2 projection of the unsheared spectrum. The integral of a one-dimensional spectrum over all frequencies is equal to the value of the first point in the time-domain. In an entirely analogous way, the projection of a two-dimensional spectrum onto the ω_2 axis is the same as the Fourier transform of the first t_1 increment. The SNR in the projection is therefore equal to the SNR of the first t_1 increment (this has been verified experimentally). This is slightly counter-intuitive as it implies that the remaining t_1 increments are not important. However, they are needed in order to map out the t_1 evolution even though they do not contribute to the intensity in the projection.

DOI: 10.1002/mrc

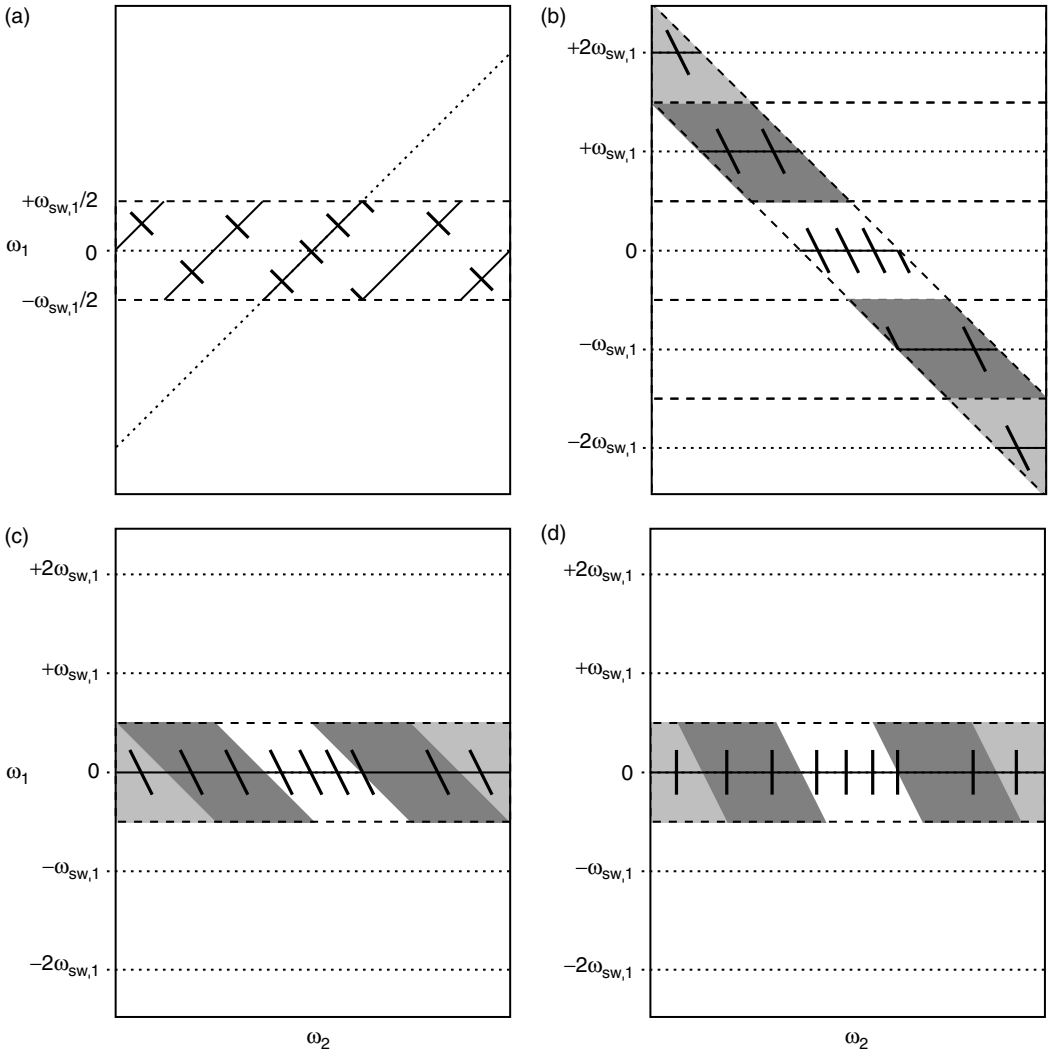

Figure 9. An illustration of the effect of shearing on the diagonal peaks of a folded spectrum. The positions of the diagonal-peak multiplets in a folded spectrum are shown in the schematic spectrum in (a). The boundaries of the spectral window are indicated by the widely-spaced dashed lines. The true diagonal, represented by the closely-spaced dashed line, is folded into a series of discrete sections, which are represented by solid lines. This spectrum is sheared parallel to ω_1, with a shear rate of -1, to give (b), transforming the rectangular spectrum into a parallelogram. Any sections of the sheared spectrum that were shifted outside the original spectral window are shaded grey. They wrap back inside, to give (c). The second shear is parallel to ω_2 with a shear rate of $\frac{1}{2}$, which gives the spectrum in (d).

The SNR in the projection is therefore given by:

$$\text{SNR(projection)} = \sqrt{n}\frac{fS}{\sigma}$$

where n is the number of scans per increment, and $f = \frac{1}{2}\sin^2\beta$ is the intensity factor that arises from the two small flip angle pulses.

A conventional proton experiment that has the *same experiment time* is acquired with nN_1 scans, and so has the following SNR:

$$\text{SNR(1D)} = \sqrt{nN_1}\,\frac{S}{\sigma}$$

The ratio of the two SNRs is therefore:

$$\frac{\text{SNR(projection)}}{\text{SNR(1D)}} = \frac{\sin^2\beta}{2\sqrt{N_1}} \qquad (14)$$

For example, if an anti z-COSY spectrum is recorded with 700 t_1 increments, and $\beta = 10^\circ$, the ratio in Eqn. 14 is equal to 5.7×10^{-4}. Generating the proton-decoupled spectrum thus incurs a heavy penalty in terms of the SNR. The use of the two small flip angle pulses is in large part responsible for this, along with a further reduction due to the large number of t_1 increments which have to be recorded.

To give a concrete example of what this implies, imagine a typical experiment in which we use 10° mixing pulses and record four transients, each taking 10 s, for each of 700 t_1 increments; this gives a total experiment time of just under 8 h. For the projection of this spectrum to have a SNR of 50 would require the SNR of a simple four transient proton spectrum to be 3000. We will see in the next section that the ω_1 spectral width can be reduced significantly, and this reduces the number of t_1 increments which are required, easily by a factor of 10. In the example above, the two-dimensional

DOI: 10.1002/mrc

spectrum needed to give a projection with an SNR of 50 could then be recorded in just under an hour. Clearly, it is very advantageous to reduce the spectral width in this way.

Where sensitivity is at a premium, the flip angle of the mixing pulses can be increased. For example, increasing them from 10° to 20° increases the signal-to-noise ratio by a factor of almost 4.

SPECTRA WITH REDUCED ω_1 SPECTRAL WIDTH

It was shown in the previous section that the linewidth in the projection is the average of the linewidths in the ω_1 and ω_2 dimensions. This means that we must acquire a sufficient number of t_1 increments so that the linewidth is determined by relaxation and not by insufficient sampling. If the ω_1 spectral width is large, say 5000 Hz, then very many t_1 increments must be recorded in order to make sure that the ω_1 linewidth is not limited by sampling. It is possible to reduce the number of required increments simply by reducing the spectral width in ω_1, but this will also result in the peaks folding in this dimension. However, it will be shown in this section that, in the sheared spectrum, the diagonal peaks will always be present in the same positions whether or not they have folded. Thus, reducing the spectral width does not affect the calculation of the projection. The cross peaks prove to be more problematic, and may fold into the region of the spectrum we wish to project. However, it will be shown that on folding they acquire different symmetry properties which allow them to be removed in a straightforward way.

As we noted above, reducing the number of increments has the effect of improving the sensitivity of the projection relative to the conventional proton spectrum, according to Eqn. 14. It is thus very desirable to reduce the ω_1 spectral width.

Diagonal peaks

When the ω_1 spectral width is reduced, the diagonal folds into discrete sections, each of which is tilted at 45° to both the ω_1 and ω_2 axes; the counter-diagonal peaks still lie on a line that is perpendicular to each section of the diagonal. This is illustrated in Fig. 9 (a). In this diagram, the central section of the diagonal has not folded, and is in its normal position. The two sections immediately to the right and left have folded once, and the two outer sections have folded twice.

The first shear (parallel to ω_1) gives the spectrum shown in (b). The central section of the diagonal shears on to $\omega_1 = 0$ as usual, while the two sections that have folded once are sheared onto the horizontal lines $\omega_1 = \pm\omega_{SW,1}$, where $\omega_{SW,1}$ is the spectral width in ω_1. The two sections that have folded twice are sheared onto $\omega_1 = \pm 2\omega_{SW,1}$. In general, there will be two sections that have folded n times (where n is an integer). One will be sheared onto $\omega_1 = +n\omega_{SW,1}$, the other will be sheared onto $\omega_1 = -n\omega_{SW,1}$. In all cases, the counter-diagonal peaks are orientated at 26.7° ($\tan^{-1}\frac{1}{2}$) to the vertical.

The rectangular spectrum has been transformed into a parallelogram. As described above, any sections of the sheared spectrum that lie outside the original spectral window are translated back inside, to reproduce a rectangular spectrum. This process is referred to as wrapping, to distinguish it from folding. A section of the diagonal that has been sheared onto $\omega_1 = +n\omega_{SW,1}$ is translated by $-n\omega_{SW,1}$ to $\omega_1 = 0$. Thus, after wrapping, the sheared spectrum is exactly the same as the one we would obtain if the diagonal had not folded, as shown in (c). Therefore, it does not matter whether or not the diagonal peaks fold, as they will always shear to the same places. Finally, the second shear aligns the multiplets so that they are parallel to ω_1, as shown in (d).

Cross peaks

It can be seen from Fig. 6 and Eqn 13 that, for a spectrum that has been acquired with the full spectral width in ω_1, the ω_2 frequency upon which the cross-peak multiplet between spins i and j is centered in the sheared spectrum is given by the average of Ω_i and Ω_j. Furthermore, cross peaks that are mirror images of each other about the diagonal in the original spectrum are symmetrically related about $\omega_1 = 0$ in the sheared spectrum. This is demonstrated for the simulated anti z-COSY spectrum of a two-spin system in Fig. 10 (a); the original spectrum and the spectra after the first and second shears are shown.

However, if as a result of reducing the spectral width the cross peaks wrap during the *first* shear, they will no longer have the symmetry properties mentioned above. Figure 10 (b) shows the original spectrum and the spectra after each shear, which are obtained when the ω_1 spectral width is set to 88% of the full spectral width; the cross peaks have not folded during acquisition, and are properly represented in the unsheared spectrum. The first shear shifts them outside of the spectral window, and so they are wrapped back inside (compare Fig. 5). As a result, the second shear shifts them to positions that are not symmetrically related about $\omega_1 = 0$.

A similar situation arises for a spectral width which is set to 53% of the full spectral width (Fig. 10 (c)). The cross peaks are shifted further outside the spectral window by the first shear, and are wrapped to positions that are closer to the diagonal peaks.

In Fig. 10 (d), the spectral width in ω_1 is 47% of the value in (a), which is sufficient for the cross and diagonal peaks at the top of the spectrum to have folded to the bottom; they now lie directly on top of the other peaks.

Setting the spectral width to 36% of the maximum value, as illustrated in Fig. 10 (e), causes all the peaks to fold once in the original spectrum. The diagonal peaks still shear to their same positions, as we expect. The cross peaks are not shifted outside the window by the first shear, but they still occupy unsymmetrical positions as they folded during the acquisition of the original spectrum.

In general, a cross-peak that is located at $(\omega_1, \omega_2) = (\Omega_1, \Omega_2)$ will be unsymmetrically related to its partner if the two peaks fold differently, either during acquisition or during the first shear. The condition for this is:

$$|\Omega_1 - \Omega_2| > \frac{1}{2}\omega_{SW,1}$$

Symmetrization

Reducing the spectral width in the ω_1 dimension has no effect on the diagonal-peak multiplets in the sheared spectrum; they are still symmetrically distributed about $\omega_1 = 0$.

DOI: 10.1002/mrc

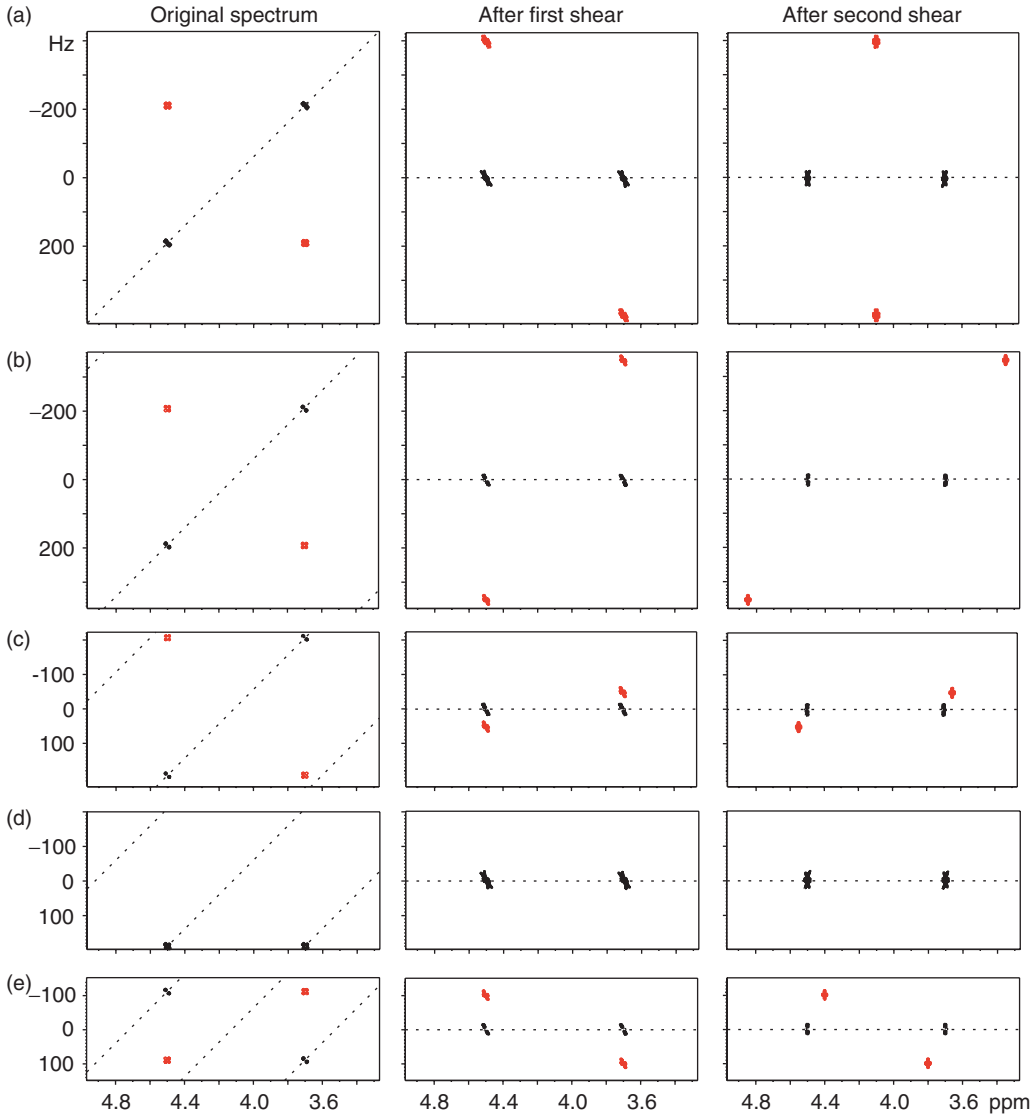

Figure 10. Simulated anti *z*-COSY spectra of a two-spin system, for different values of the spectral width in ω_1. The spectral width in the ω_2 dimension is 850 Hz in all cases. The ω_1 spectral width takes the following values: (a) 850 Hz, (b) 750 Hz, (c) 450 Hz, (d) 400 Hz, and (e) 300 Hz. The diagonal is shown as a dashed line. Where they are clearly separated from the diagonal peaks, the cross peaks have been colored red.

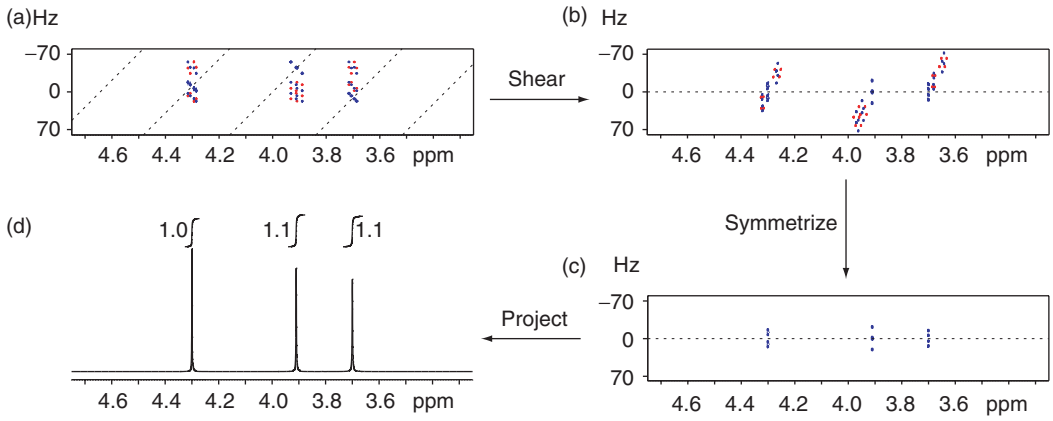

Figure 11. Illustration of the shearing and symmetrizing processes on the simulated spectrum of a three-spin system with reduced ω_1 spectral width. The folded spectrum in (a) is sheared to give the spectrum shown in (b). Symmetrization removes the cross peaks to give the spectrum in (c), which is then projected onto ω_2 to give (d). The integrals are given with the projection.

The cross-peak multiplets, if they have wrapped or folded as described above, are no longer symmetrically related to their partners. Therefore, they can be removed by applying the following symmetrization procedure to the sheared spectrum. The intensity at (ω_1, ω_2) is compared with the intensity at $(-\omega_1, \omega_2)$; the highest absolute value is replaced by the lowest absolute value, while retaining the original sign.

If there is no accidental overlap between the individual cross- and diagonal-peak multiplets, this simple symmetrization procedure removes all of the cross peaks that have wrapped or folded differently from their partners, and leaves the diagonal peaks unaffected. The procedure is remarkably effective at cleaning up the spectrum, as is shown in Fig. 11.

Cross peaks which have not wrapped differently from their partners are symmetrically placed about $\omega_1 = 0$, and so are not suppressed. Such cross peaks necessarily lie close to the diagonal of the original anti *z*-COSY spectrum, and, as has been commented on before, are analogous to the strong coupling artifacts seen in two-dimensional *J*-spectra.

If, as a result of the folding in ω_1, an individual *component* of a cross-peak multiplet falls on top of an individual *component* of a diagonal-peak multiplet, then the intensity of the latter will be perturbed in a way which is not necessarily removed by the symmetrization process. If the diagonal peak is reduced in intensity by the overlapping cross-peak, the symmetrization will transfer the perturbation in one component of the diagonal-peak multiplet to its symmetry-related counterpart. If, on the other hand, the diagonal peak component is increased in intensity, the symmetrization will restore its correct intensity.

The result of all this is that, even after symmetrization, the folding of the cross peaks into the region occupied by the diagonal peaks can lead to intensity perturbations which will affect both the projection and the multiplets. The former is seen in Fig. 11, in the form of the perturbation of the integrals of the projection.

If the linewidths in the two dimensions are the same, the symmetrization process affects neither the lineshape nor the linewidth in the projection. However, if the ω_1 linewidth is greater than the ω_2 linewidth, which may be the case due to restricted sampling in t_1, the symmetrization process results in changes in the lineshape of the spectrum and its projection. Generally speaking, the peaks in the projected spectrum have a linewidth at half-height which is close to the ω_2 linewidth. However, the base of the lineshape is characteristic of the broader line in the ω_1 dimension. Therefore, in practice there is little real improvement in resolution.

A useful side effect of the symmetrization process is an improvement of the SNR of the projection by approximately $\sqrt{2}$ when compared to the SNR of the projection of the unsymmetrized spectrum.

EXPERIMENTAL VERIFICATION

In this section, the method for obtaining a proton-decoupled proton spectrum is illustrated experimentally with the spectra of camphor, whose structure is shown in Fig. 12.

All of the spectra in this section were recorded at 500 MHz for protons on a Bruker Avance DRX500 spectrometer. (The pulse sequences that were used to acquire the spectra, and the AU programs that were used for the shearing and symmetrization operations are available on the WWW at http://www-keeler.ch.cam.ac.uk.) Both mixing pulses had the same flip angle of 10°. Selection of the CTP was achieved by a homospoil gradient during the *z*-filter (50% of the maximum intensity of 59.5 G cm^{-1}, 5 ms, half-sine shape). The swept pulse that was used to suppress the zero-quantum artifacts was an adiabatic CHIRP 180° pulse with a radiofrequency field strength of 1.7 kHz, which was swept through an offset range of 24 kHz in 24 ms. The accompanying gradient had a strength of 4% of the maximum. A two-step phase cycle in which the phases of the first pulse and receiver were simultaneously changed by 180° was used to suppress the axial peaks. The spectral width in ω_2 is 1085 Hz, and the spectra were processed using the

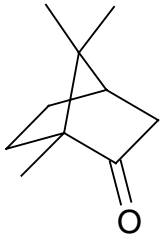

Figure 12. The structure of camphor.

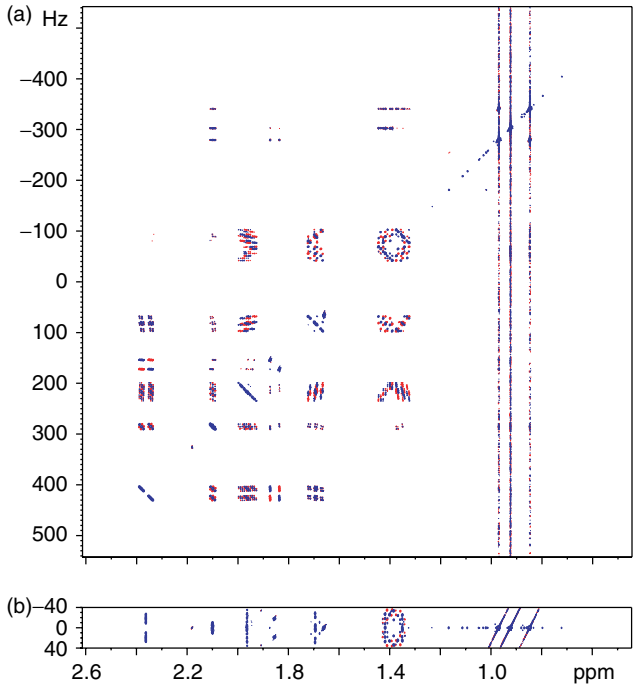

Figure 13. The anti *z*-COSY spectrum of camphor is shown in (a). The spectrum is sheared, and the central region, which is shown in (b), is the part projected to give the decoupled spectrum. The region between 1.35 and 1.42 ppm contains a pair of cross-peak multiplets that lie very close to the diagonal, so they are included in the projected region. There is also some t_1 noise visible at the chemical shifts of the three methyl groups (0.8 to 1.0 ppm). The spectral width in ω_1 is 1085 Hz; 760 t_1 increments were recorded giving a maximum value of t_1 of 0.7 s.

DOI: 10.1002/mrc

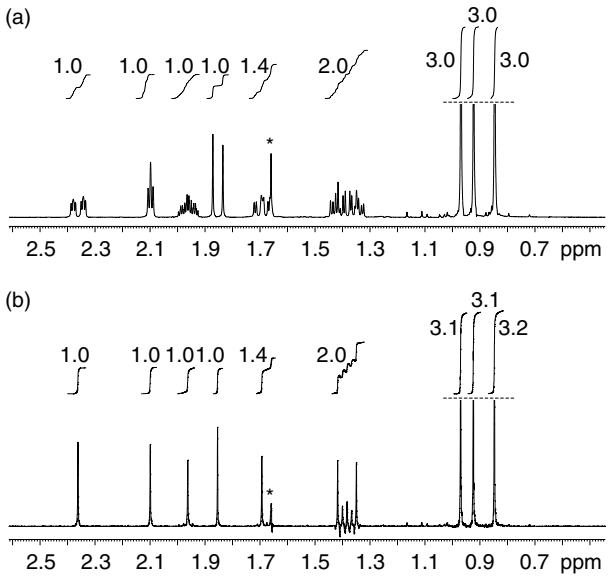

Figure 14. The conventional proton spectrum of camphor is shown in (a). The projection of the anti *z*-COSY spectrum from Fig. 13 is shown in (b). For both spectra, the integrals of the peaks are given relative to the resonance from the proton at 2.36 ppm. The peak at 1.66 ppm is due to an impurity, and is marked with a star. The two peaks at 1.35 ppm and 1.42 ppm are due to spins that are strongly coupled to each other. The result is that the cross peaks lie very close to the diagonal (see Fig. 13) and project to give the set of anti-phase peaks between the two singlet peaks at 1.35 ppm and 1.42 ppm.

States–Haberkorn–Ruben method.[11] The acquisition time in t_2 was 1.89 s.

The anti *z*-COSY spectrum of camphor with the full spectral width of 1085 Hz in ω_1 is shown in Fig. 13(a), and the region of the doubly sheared spectrum that is projected to give the decoupled spectrum is shown in (b). The projection is shown in Fig. 14 (b), with the conventional proton spectrum in (a) for comparison. The multiplet structures of the first seven camphor multiplets (starting at the largest chemical shift) obtained from the vertical cross-sections taken at the offsets of the spins are shown in Fig. 15(a)–(g).

The multiplets shown in (f) and (g) are of particular interest as they overlap in the conventional proton spectrum, making it impossible to distinguish their form. This overlap is completely removed in the sheared anti *z*-COSY spectrum due to the separation of offset and coupling information, giving a clear view of the multiplets.

The cross-peak multiplets between the diagonal-peak multiplets that are centered at 1.42 ppm and 1.35 ppm lie very close to the diagonal, and so have to be included in the region that is projected. These cross peaks project to the anti-phase peaks between the two singlets visible in Fig. 14(b). These extra peaks can be left out of the projection by summing over a smaller range of frequencies in ω_1. A series of 'limited projections' of the sheared camphor anti *z*-COSY spectrum are shown in Fig. 16(a)–(c).

Such an approach will, of course, produce decoupled spectra in which the integrals are distorted as not all the diagonal peaks are included in the projection. Nevertheless, these limited projections may be of interest as they avoid any contributions from the cross peaks.

An anti *z*-COSY spectrum of camphor in which the ω_1 spectral width has been reduced to 100 Hz is shown in Fig. 17(a), and the sheared spectrum is shown in (b). It can be seen that the diagonal-peak multiplets have sheared to the same positions as in Fig. 13(b). However, the cross peaks have folded and so lie all over the spectrum. As was discussed above, the majority of the cross peaks are not symmetrically displaced about $\omega_1 = 0$, and so can be removed by applying a symmetrization procedure; this gives the spectrum shown in (c). The cross peaks between 1.35 and 1.42 ppm lie close to the diagonal and so have not wrapped differently to their partners in this spectrum. As a result, they are not removed by the symmetrization procedure.

DIRECT SUPPRESSION OF THE CROSS PEAKS

Rather than relying solely on the symmetrization procedure for the elimination of the cross peaks, it would be useful to have a pulse-sequence based method for suppressing them. We term this 'direct' suppression of the cross peaks.

Suppressing the cross peaks in an anti *z*-COSY experiment is essentially the same problem as the suppression of zero-quantum coherence during a *z*-filter,[7,8,12] or the removal of strong coupling artifacts from a *J*-spectrum.[13] In both cases, the wanted and the unwanted magnetization terms follow

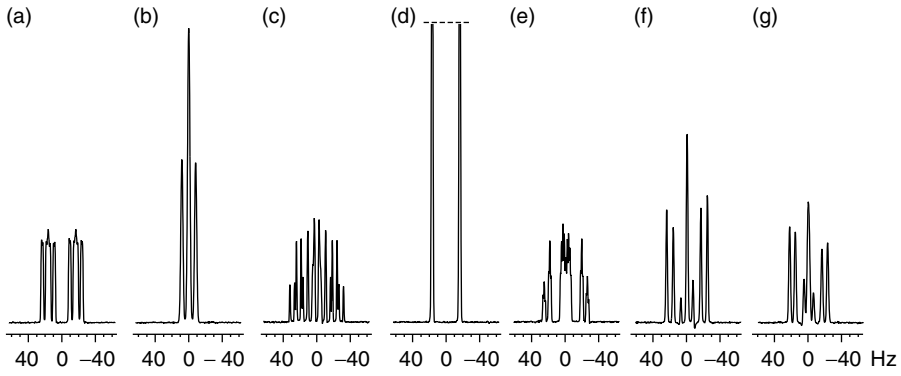

Figure 15. Cross-sections taken from Fig. 13(b) giving the structures of the seven camphor multiplets with the largest chemical shifts. The cross-sections are taken at the following shifts: (a) 2.36 ppm, (b) 2.10 ppm, (c) 1.96 ppm, (d) 1.85 ppm, (e) 1.69 ppm, (f) 1.42 ppm, and (g) 1.35 ppm.

DOI: 10.1002/mrc

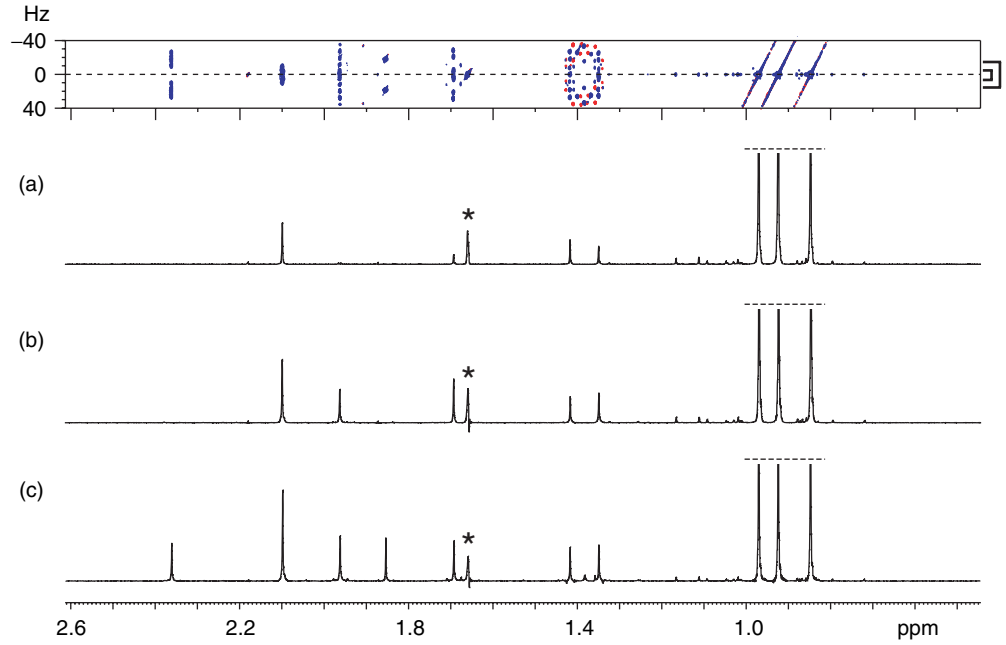

Figure 16. Successive limited projections of the region containing the diagonal-peak multiplets in the sheared spectrum of camphor. Spectrum (a) is the single row at $\omega_1 = 0$ (dashed line). The close-lying cross peaks do not contribute any intensity to this spectrum. However, some of the diagonal peaks are not included either, as they also have zero intensity in this row. Widening the range of the limited projection to 11 Hz (range indicated by the smaller square bracket on the right hand side of the two-dimensional spectrum) includes more of the diagonal-peak intensity, giving the spectrum in (b). Increasing the range to 33 Hz (range indicated by the larger square bracket) gives a spectrum in which all the diagonal-peak multiplets contribute some intensity, as shown in (c). However, part of the close-lying cross-peak multiplet is also included. The peak labelled with the star is an impurity.

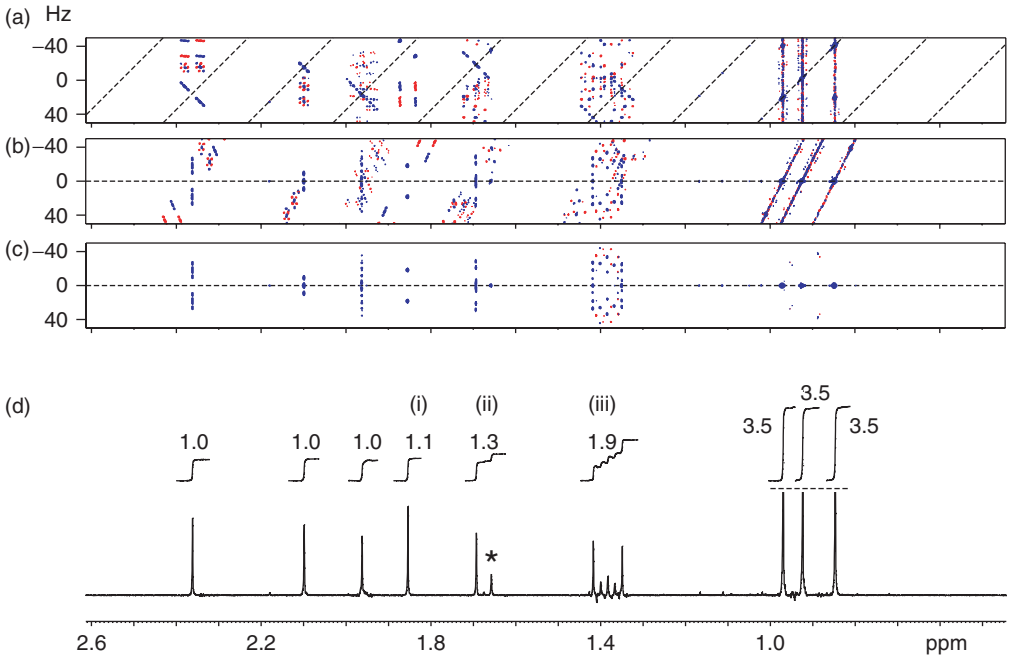

Figure 17. The anti *z*-COSY spectrum of camphor with reduced ω_1 spectral width. The spectrum is sheared to give (b), and after symmetrization gives spectrum (c). This spectrum is then projected to give the decoupled spectrum in (d). The integrals are still in very good agreement with those from the conventional spectrum, but there is some deviation for the integrals labelled (i)–(iii); the peak labelled with the star is an impurity. The close-lying cross peaks between 1.35 and 1.42 ppm are still present in (c), as they are symmetrically distributed in the sheared spectrum, and so they contribute to the projection. The spectral width in ω_1 is 100 Hz, and 70 t_1 increments were recorded, giving a maximum value of t_1 of 0.7 s.

DOI: 10.1002/mrc

the same CTP, and so cannot be separated by conventional phase-cycling or gradient selection methods. However, there is a crucial difference between cross-peak and diagonal-peak terms that allows the former to be suppressed. This is that the cross peaks are produced by coherence that is transferred from one spin to another during the mixing period: the magnetization therefore evolves at a different offset either side of the *z*-filter. In contrast, the diagonal peak terms evolve at the same offset throughout the pulse sequence.

Figure 18 shows modified anti *z*-COSY pulse sequences that exploit this difference between the fate of magnetization leading to cross and diagonal peaks in order to suppress the former. A delay δ is inserted either side of the mixing period, and a CTP is selected such that the coherence order is of *opposite* sign during the two delays. As a result, for a diagonal peak the phase acquired during the first delay δ is equal and opposite to that acquired during the second delay δ. Thus, diagonal peaks acquire no phase due to the two delays. In contrast, magnetization giving rise to a cross-peak between spins i and j will acquire a phase $-\Omega_i\delta$ during the first delay, and $\Omega_j\delta$ during the second delay. Thus, cross peaks acquire an overall phase of $(\Omega_j - \Omega_i)\delta$, and so can be suppressed by the co-addition of spectra recorded with different values of δ.

In order that the magnetization that gives rise to the diagonal peaks acquires no phase as a function of δ, the coherence must be ±1 during the first delay, and ∓1 during the second delay. Thus, the resulting spectrum will have phase-twist lineshapes. In order to recover absorption mode spectra, P- and N-type spectra must be recorded and combined in the usual way. The two variants of the pulse sequence needed to record the N- and P-type spectra are shown in Fig. 18(a) and (b), respectively. Note the inclusion of an extra 180° pulse in (b) just prior to acquisition.

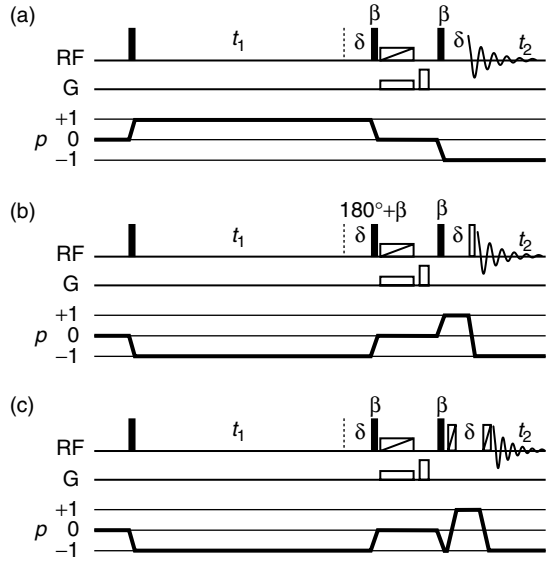

Figure 18. Anti *z*-COSY pulse sequences incorporating the multiple-scan cross-peak suppression scheme. The required CTPs are also included. The sequence shown in (a) gives the N-type spectrum, and the sequence shown in (b) gives the P-type spectrum. The open rectangle in (b) represents a hard 180° pulse. Sequence (c) also gives the P-type spectrum, but has been modified to include a pair of composite pulses (the two open rectangles with diagonal strokes flanking the second delay δ).

Analysis of the pulse sequences

In this section we will analyze the modified pulse sequences of Fig. 18; it is sufficient to confine the discussion to a two-spin system, as this illustrates all the relevant features of this method for suppressing the cross peaks. Starting with equilibrium magnetization on spin one, the 90° pulse generates $-\hat{I}_{1y} = \frac{1}{2}\mathrm{i}(\hat{I}_{1+} - \hat{I}_{1-})(\hat{I}_{2\alpha} + \hat{I}_{2\beta})$, which represents equal amounts of coherence of order +1 and −1. The operator $\hat{I}_{1+}$ ultimately produces the N-type spectrum, whereas $\hat{I}_{1-}$ gives the P-type spectrum. For simplicity, we will calculate the evolution of the single operator $\hat{I}_{1+}\hat{I}_{2\alpha}$ during the N-type pulse sequence (a), and then do the same for the complementary operator $-\hat{I}_{1-}\hat{I}_{2\alpha}$ during the P-type pulse sequence (b).

If we assume that the delay δ is short enough for *J*-modulation to be insignificant ($\delta \ll 1/|J_{12}|$), the operator $\hat{I}_{1+}\hat{I}_{2\alpha}$ evolves to give the following term just prior to the mixing period:

$$\hat{I}_{1+}\hat{I}_{2\alpha}\exp[-\mathrm{i}(\Omega_1 + \pi J_{12})t_1]\exp[-\mathrm{i}\Omega_1\delta]$$

The population terms generated by the first β pulse are:

$$\frac{1}{2}\mathrm{i}\sin\beta\cos^2\frac{1}{2}\beta(\hat{I}_{1\alpha}\hat{I}_{2\alpha} - \hat{I}_{1\beta}\hat{I}_{2\alpha})\exp[-\mathrm{i}(\Omega_1 + \pi J_{12})t_1] \times \exp[-\mathrm{i}\Omega_1\delta]$$

where, as before, it has been assumed that β is small. The swept 180° pulse interconverts $\hat{I}_{i\alpha}$ and $\hat{I}_{i\beta}$ to give:

$$\frac{1}{2}\mathrm{i}\sin\beta\cos^2\frac{1}{2}\beta(\hat{I}_{1\beta}\hat{I}_{2\beta} - \hat{I}_{1\alpha}\hat{I}_{2\beta})\exp[-\mathrm{i}(\Omega_1 + \pi J_{12})t_1] \times \exp[-\mathrm{i}\Omega_1\delta]$$

The second β pulse then produces the following observable terms of coherence order −1:

$$-\frac{1}{4}\sin^2\beta\cos^4\frac{1}{2}\beta(2\hat{I}_{1-}\hat{I}_{2\beta} + \hat{I}_{1\beta}\hat{I}_{2-} - \hat{I}_{1\alpha}\hat{I}_{2-}) \times \exp[-\mathrm{i}(\Omega_1 + \pi J_{12})t_1]\exp[-\mathrm{i}\Omega_1\delta]$$

this term comprises one diagonal peak and two cross peaks. Finally, evolution during the second δ delay gives:

diagonal peak

$$-\frac{1}{2}\sin^2\beta\cos^4\frac{1}{2}\beta\exp[-\mathrm{i}(\Omega_1 + \pi J_{12})t_1]\hat{I}_{1-}\hat{I}_{2\beta}$$

cross-peak

$$-\frac{1}{4}\sin^2\beta\cos^4\frac{1}{2}\beta\exp[\mathrm{i}(\Omega_2 - \Omega_1)\delta]\exp[-\mathrm{i}(\Omega_1 + \pi J_{12})t_1]\hat{I}_{1\beta}\hat{I}_{2-}$$

cross-peak

$$+\frac{1}{4}\sin^2\beta\cos^4\frac{1}{2}\beta\exp[\mathrm{i}(\Omega_2 - \Omega_1)\delta]\exp[-\mathrm{i}(\Omega_1 + \pi J_{12})t_1]\hat{I}_{1\alpha}\hat{I}_{2-}$$

Note that the cross peaks acquire a phase that is dependent on δ, whereas the diagonal peak does not.

In the P-type experiment, the operator $-\hat{I}_{1-}\hat{I}_{2\alpha}$ produces the following observable terms:

diagonal peak

$$-\frac{1}{2}\sin^2\beta\cos^4\frac{1}{2}\beta\exp[\mathrm{i}(\Omega_1+\pi J_{12})t_1]\hat{I}_{1-}\hat{I}_{2\beta}$$

cross-peak

$$-\frac{1}{4}\sin^2\beta\cos^4\frac{1}{2}\beta\exp[-\mathrm{i}(\Omega_2-\Omega_1)\delta]\exp[\mathrm{i}(\Omega_1+\pi J_{12})t_1]\hat{I}_{1\beta}\hat{I}_{2-}$$

cross-peak

$$+\frac{1}{4}\sin^2\beta\cos^4\frac{1}{2}\beta\exp[-\mathrm{i}(\Omega_2-\Omega_1)\delta]\exp[\mathrm{i}(\Omega_1+\pi J_{12})t_1]\hat{I}_{1\alpha}\hat{I}_{2-}$$

Again, it is only the cross-peak terms which have acquired a phase which depends on δ.

If two experiments are acquired, the first with $\delta = 0$ and the second with $\delta = \pi/|\Omega_1 - \Omega_2|$, the cross peaks will have different signs in each experiment, whereas the diagonal peaks will be unaltered. Adding the two experiments will therefore eliminate the cross peaks. If there are several cross-peak multiplets that need to be suppressed, the experiment is repeated a number of times (typically eight) with a systematic variation of δ.[12] The sum of the resulting data will produce a spectrum with a net attenuation of the intensities of the cross peaks.

The above analysis is valid only if the evolution of coupling during δ can be ignored, i.e. δ is small. Such small values can be used to suppress cross peaks that lie far from the diagonal in the unfolded spectrum. However, cross peaks that lie closer to the diagonal, and are therefore associated with smaller values of $|\Omega_1 - \Omega_2|$, can be suppressed only with larger values of the delay. In most practical cases, δ is likely to extend to values such that we must take into account the evolution of the coupling. The effect of this evolution on the diagonal peaks will now be calculated.

In the N-type experiment, the operator $\hat{I}_{1+}\hat{I}_{2\alpha}$ evolves during the first delay δ to give:

$$\hat{I}_{1+}\hat{I}_{2\alpha} \xrightarrow{\hat{H}_{\mathrm{free}}\delta} \hat{I}_{1+}\hat{I}_{2\alpha}\exp[-\mathrm{i}(\Omega_1+\pi J_{12})\delta].$$

The z-filter comprises two small flip angle pulses and a swept 180° pulse, so its overall effect is to change the polarization of the passive spin; appropriate coherence selection is also used to ensure that the coherence order is changed to -1. The resulting diagonal-peak term is therefore

$$-\frac{1}{2}\sin^2\beta\cos^4\frac{1}{2}\beta\exp[-\mathrm{i}(\Omega_1+\pi J_{12})\delta]\hat{I}_{1-}\hat{I}_{2\beta}$$

This term evolves during the second delay δ to give:

$$\begin{aligned}&-\frac{1}{2}\sin^2\beta\cos^4\frac{1}{2}\beta\exp[-\mathrm{i}(\Omega_1+\pi J_{12})\delta]\\&\quad\times\exp[\mathrm{i}(\Omega_1-\pi J_{12})\delta]\hat{I}_{1-}\hat{I}_{2\beta}\\&\quad=-\frac{1}{2}\sin^2\beta\cos^4\frac{1}{2}\beta\exp[-2\mathrm{i}\pi J_{12}\delta]\hat{I}_{1-}\hat{I}_{2\beta}\end{aligned}$$

We see that the combination of the delays and the z-filter results in a refocusing of the offset, but the coupling evolves for 2δ. Therefore, in the N-type spectrum, the diagonal peaks acquire a phase error due to the J-modulation during the two delays δ.

The complementary operator in the P-type experiment, $-\hat{I}_{1-}\hat{I}_{2\alpha}$, evolves during the first delay δ to give:

$$-\hat{I}_{1-}\hat{I}_{2\alpha}\exp[\mathrm{i}(\Omega_1+\pi J_{12})\delta]$$

The z-filter now comprises two small flip angle pulses and *two* 180° pulses (the first mixing pulse has flip angle $180^\circ + \beta$). Each 180° pulse changes the polarization of the passive spin, and so together they have no net effect. Therefore, the z-filter does *not* change the polarization of the passive spin. The coherence order does change sign, however, giving the following diagonal-peak term just after the mixing period:

$$-\frac{1}{2}\sin^2\beta\cos^4\frac{1}{2}\beta\exp[\mathrm{i}(\Omega_1+\pi J_{12})\delta]\hat{I}_{1+}\hat{I}_{2\alpha}$$

This term evolves during the final delay δ to give:

$$\begin{aligned}&-\frac{1}{2}\sin^2\beta\cos^4\frac{1}{2}\beta\exp[\mathrm{i}(\Omega_1+\pi J_{12})\delta]\\&\quad\times\exp[-\mathrm{i}(\Omega_1+\pi J_{12})\delta]\hat{I}_{1+}\hat{I}_{2\alpha}=-\frac{1}{2}\sin^2\beta\cos^4\frac{1}{2}\beta\hat{I}_{1+}\hat{I}_{2\alpha}\end{aligned}$$

The sequence of the delays and the z-filter refocuses both the offset *and* the scalar coupling; as a result, the diagonal peak terms in the P-type experiment are completely unaffected by the value of the delay δ.[14]

This J-modulation of the N-type, but not of the P-type, spectrum is a problem as it results in a phase distortion when the two spectra are combined, i.e. the spectrum, and hence the projection, will not be in the absorption mode. We conclude, therefore, that the method cannot be used to suppress cross peaks that lie close to the diagonal, as the values of δ that would be required would result in significant phase distortions.

A further problem will arise when δ is long enough that transverse relaxation is significant. There will be reductions in intensity by a factor of $\exp[-2\delta/T_2]$, which is dependent upon the transverse relaxation time constant T_2. The peak heights will therefore gain a relaxation weighting, which will distort the integrals of the projection.

Experimental results

The method for the direct suppression of the cross peaks is illustrated with the spectra of camphor. Eight equally spaced values of the delay δ between 0 and 10 ms were used to suppress the cross peaks: the minimum offset difference that can be suppressed with this choice of delays is 87.5 Hz. A four-step phase cycle was used in which the phase of the first mixing pulse took the values $[x, y, -x, -y]$ in the N-type experiment, and $[x, -y, -x, y]$ in the P-type experiment: the receiver phase was $[x, y, -x, -y]$ in both experiments, thus selecting $\Delta p = -1$ in the former, and $+1$ in the latter.

Rather than using a single hard 180° pulse at the end of the P-type sequence, it is recommended that a pair of composite pulses, which have a greater tolerance of radiofrequency field inhomogeneity, are used, as shown in Fig. 18(c). The spectra presented in this section were recorded using this sequence in which the composite broadband inversion pulses (BIPs)

DOI: 10.1002/mrc

were those described by Smith *et al*.[15] It is necessary to use two such pulses so that the phase errors produced by the first are cancelled by the second. Both BIPs had a pulse length of 100 μs, and a B_1 field of 20 kHz. All other acquisition parameters are the same as those given for the spectra in Figs 13 and 17.

Figure 19 shows the anti *z*-COSY spectrum that was acquired with the full spectral width in ω_1. There is a significant reduction in the intensity of the cross peaks, although those lying close to the diagonal between 1.35 and 1.42 ppm are only partially suppressed on account of the small difference in the offsets of the coupled spins.

Since the suppression requires recording spectra with multiple values of δ, a large minimum experiment time is needed, limiting the resolution that can be obtained in ω_1.

As before, this problem can be solved by reducing the spectral width in this dimension. The resulting spectrum is shown in Fig 20(a), which also shows an excellent degree of cross-peak suppression. The sheared spectrum is shown in (b), and this is projected to give the decoupled spectrum in (c). There is some deviation in the values of the integrals, which is attributed to transverse relaxation during the delays δ. It can also be seen that the residual cross-peak intensity leads to some small distortions visible near the bases of the peaks. This unwanted intensity can be removed by symmetrizing the spectrum in (b), and then projecting to give the cleaner spectrum in (d).

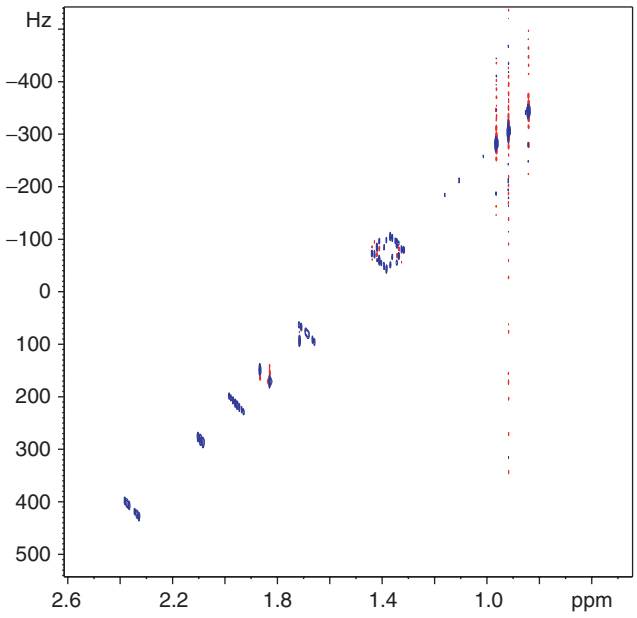

Figure 19. The anti *z*-COSY spectrum of camphor recorded using the pulse sequences of Fig. 18 which are modified for the suppression of the cross peaks using variable delays. The delay δ took eight equally spaced values between 0 and 10 ms. All the cross peaks that lie well away from the diagonal have been suppressed significantly. The close-lying cross peaks between 1.35 and 1.42 ppm are, however, still present. The spectral width in ω_1 is 1085 Hz, and 70 t_1 increments were recorded giving a maximum value of t_1 of 64 ms. Gaussian multiplication was used in the indirect dimension. The total experiment time was 16 h.

It was pointed out before that if there is any overlap between a component of a cross-peak multiplet and a component of a diagonal-peak multiplet, there may be a distortion in the intensity of the latter on symmetrizing the spectrum. This effect is, of course, reduced when the cross peaks have been suppressed directly.

APPLICATIONS

There are a number of experiments in which it would be advantageous to have access to a proton-decoupled proton spectrum. Three such applications are presented in this section.

Diffusion measurements

Diffusion-ordered spectroscopy (DOSY) is used to separate the components of a mixture which have different diffusion constants.[16] A basic pulse sequence for a diffusion-weighted anti *z*-COSY experiment is shown in Fig. 21(a).

A stimulated echo is inserted before t_1, which includes two diffusion gradients of duration δ and strength G, and which are separated by a delay Δ. The diffusion-dependent signal attenuation is given by the well-known formula:[17]

$$S = S_0 \exp[-D\gamma^2 s^2 G^2 \delta^2 \Delta_r] \qquad (15)$$

where S is the intensity of the attenuated signal, S_0 is the signal intensity in the absence of diffusion, D is the diffusion constant, γ is the gyromagnetic ratio of the nucleus, s is a shape factor which compensates for nonrectangular gradient shapes, and Δ_r is a reduced delay time.

A series of anti *z*-COSY spectra are recorded for a range of values of G. Each spectrum is then sheared, symmetrized, and projected in the usual way to give a set of decoupled spectra that are diffusion-weighted. The intensities of the peaks are measured and fitted to Eqn 15 to determine the diffusion constant D.

This method is illustrated with a mixture of 15 mg of quinine, 11 mg of geraniol, and 13 mg of camphene in 1 ml of MeOD. The structures of the three molecules are shown in Fig. 22. The sample temperature was 300 K, and the heating gas flow rate was 400 l h^{-1}. Eight diffusion-weighted spectra were acquired, with equally spaced gradient strengths between 10% and 50% of the maximum. The diffusion gradient duration δ and inter-gradient delay Δ were 2 and 150 ms, respectively. Coherence order zero was selected during the first *z*-filter with a homospoil (37%, 2 ms). All gradient pulses were shaped to a half-sine bell. The phase cycle comprised two steps in which the phases of the third 90° pulse and receiver were simultaneously changed by 180°. The spectral widths in ω_1 and ω_2 are 100 and 4496 Hz, respectively. The acquisition time in t_2 was 1.82 s; 70 t_1 increments were recorded, giving a maximum value of t_1 of 0.7 s. The effects of convection were reduced by spinning the sample about the *z*-axis.[18]

The conventional proton spectrum is shown in Fig. 23(a), with the projection of the sheared anti *z*-COSY spectrum in (b). There is a good separation of the peaks above about 2 ppm in the former, but in the range 1 to 2 ppm, the spectrum is more crowded.

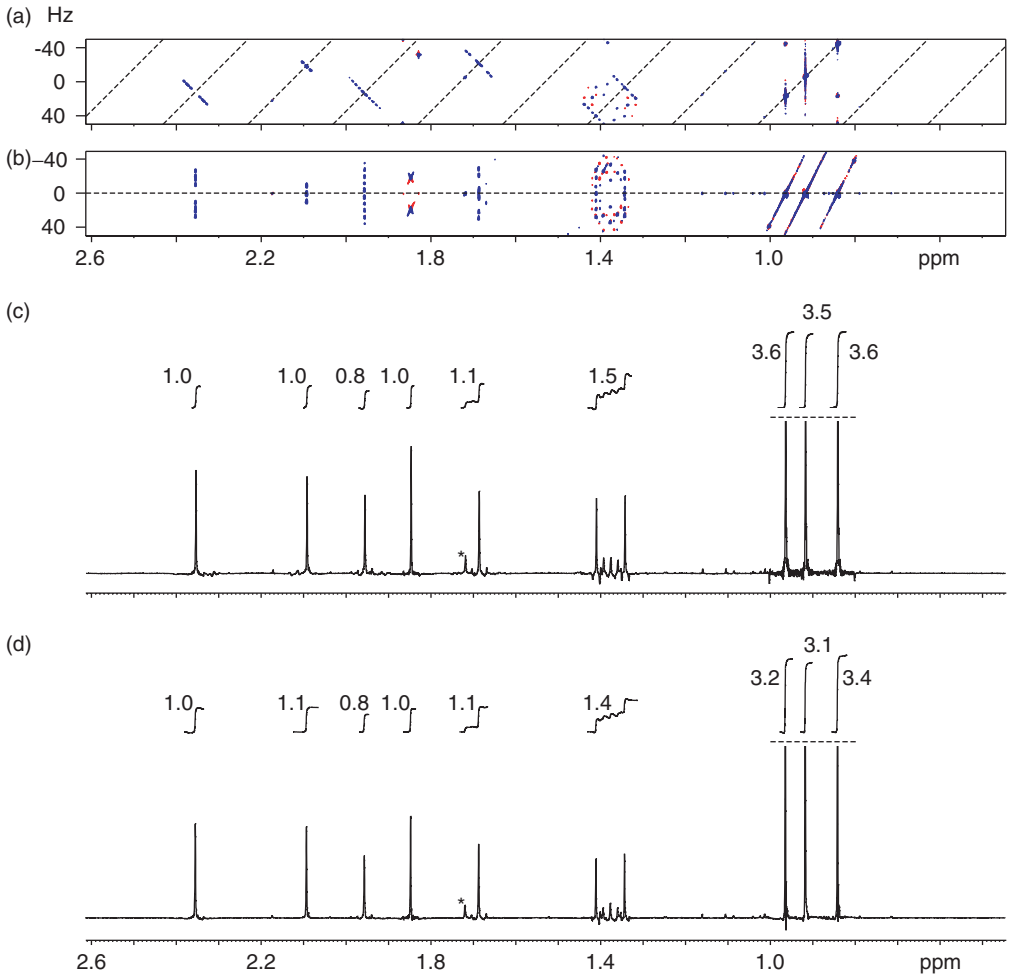

Figure 20. The anti *z*-COSY spectrum of camphor recorded with reduced ω_1 spectral width and the variable delay cross-peak suppression scheme of Fig. 18. The folded spectrum is shown in (a). This is sheared to give the spectrum in (b), which is then projected to give the decoupled spectrum in (c). The integrals are given relative to the peak on the far left. There is some deviation from the values in the conventional spectrum due to differential transverse relaxation during the variable delays. Some residual cross-peak intensity is present, which is removed by symmetrization of the sheared spectrum in (b). The projection of this symmetrized spectrum is shown in (d). The impurity peak in each decoupled spectrum is labelled with a star: it is in a different position to that in Fig. 14. The spectral width in ω_1 is 100 Hz, and 70 t_1 increments were recorded, giving a maximum value of t_1 of 0.7 s. The values of the delay δ and the total experiment time are the same as for the spectrum in Fig. 19.

It is in this region that we expect to see significant advantages from analyzing the decoupled, rather than the regular, spectra.

Figure 24 shows expansions of this crowded region of the spectra; the improved separation offered by the decoupled spectrum is evident. Shown in (c) is the DOSY spectrum computed from a series of diffusion-weighted decoupled spectra. The diffusion coefficient for each peak in the spectrum was determined, and then this value was represented in the two-dimensional DOSY spectrum by a Gaussian line whose width is proportional to the standard error of the fit.

From other well-resolved peaks in the spectrum it is possible to determine the average diffusion coefficients of the three components. These values are indicated by the dashed lines. We see that even in this crowded region, there is a clear separation of the majority of the peaks according to their diffusion coefficient.

Longitudinal relaxation measurements

Figure 21(b) shows an anti *z*-COSY pulse sequence that has been modified to give a T_1 relaxation weighting to the intensities of the peaks in the two-dimensional spectrum. The equilibrium magnetization is inverted by a BIP, and is allowed to relax during the subsequent delay τ. The signal intensity is given by:

$$S = S_0(1 - 2\exp[-\tau/T_1]) \qquad (16)$$

where S_0 is the intensity arising from a simple 90° pulse.

The procedure for determining the values of T_1 using the pulse sequence in (b) is analogous to determining a diffusion constant: a series of spectra is recorded with a systematic variation of τ; these are then sheared, symmetrized, and projected, and the peak intensities are fitted to Eqn 16.

The experimental data that were collected confirm that the relaxation-weighted decoupled spectra that are thus generated can be used to accurately determine the values of T_1 for each proton.

DOI: 10.1002/mrc

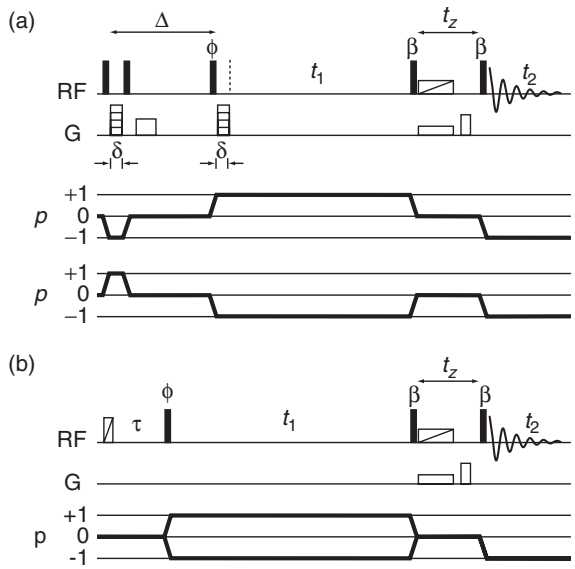

Figure 21. Anti *z*-COSY pulse sequences and CTPs that have been modified for diffusion and T_1 relaxation measurements. The sequence shown in (a) produces an anti *z*-COSY spectrum in which the peaks have diffusion-weighted intensities. The two CTPs give the N-type and P-type spectra respectively. The sequence in (b) produces a spectrum in which the intensities are weighted by the degree of T_1 relaxation during the delay τ. The first pulse with the diagonal stroke in (b) is a BIP.[15] In both experiments, all the pulses are of phase *x*, and the axial peaks are suppressed by phase-cycling the pulses labelled ϕ and the receiver according to $[x, -x]$.

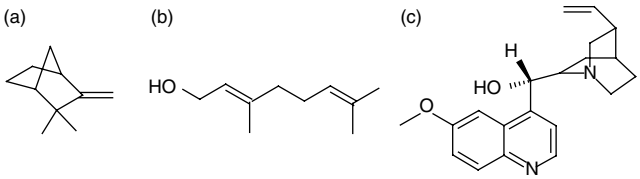

Figure 22. The structures of the three components of the mixture. Camphene is shown in (a), geraniol is shown in (b), and quinine is shown in (c).

Analysis of a complex mixture

A further application of this method of recording a decoupled spectrum is in the analysis of complex mixtures, such as those which arise from the study of metabolism.[19] We demonstrate this with the spectra of a sample of a KG1a (AML cancer model) cell extract kindly supplied by Dr Ulrich Günther at the University of Birmingham. The anti *z*-COSY spectrum with reduced ω_1 spectral width of this sample (in D_2O) was recorded, with presaturation of the residual water signal. As sensitivity was at a premium, the flip angle of the mixing pulses was set to 20°; the data were acquired with 80 scans per increment using a cryo probe. The spectral widths in ω_1 and ω_2 are 100 Hz and 5000 Hz respectively; the acquisition time in t_2 was 0.8 s, and the number of increments in the indirect dimension was 40, giving a maximum value of t_1 of 0.4 s. The spectrum was processed with a decaying exponential weighting function with 1.3 Hz of line broadening in both dimensions.

The conventional proton spectrum of the sample is shown in Fig. 25 (a), and the projection of the sheared and symmetrized anti *z*-COSY spectrum is shown in (b).

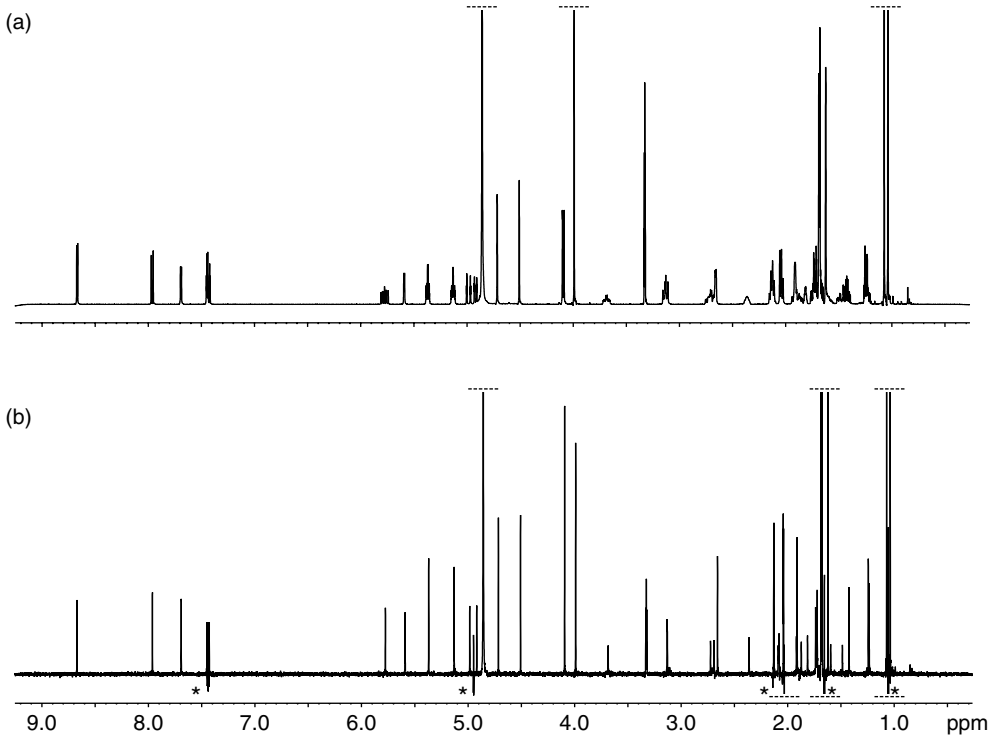

Figure 23. The decoupled spectrum of the mixture of quinine, geraniol, and camphene in MeOD. The conventional proton spectrum is shown in (a), and the projection of the sheared anti *z*-COSY spectrum is shown in (b). Any multiplet structures in the latter that are due to close-lying cross-peak multiplets are labelled with a star.

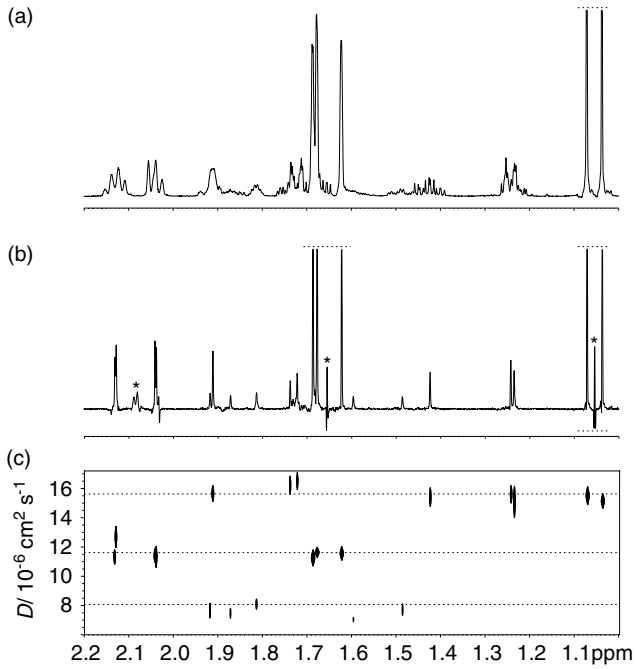

Figure 24. Illustration of the use of decoupled proton spectra to generate a two-dimensional DOSY spectrum of a crowded region from the spectrum of a mixture of quinine, geraniol, and camphene in MeOD. The conventional proton spectrum is shown in (a), and shows several overlapping multiplets. The decoupled spectrum, which shows considerable simplification, is shown in (b). There are three sets of peaks which correspond to the projection of close-lying cross peaks; these are indicated by a star. The two-dimensional decoupled DOSY spectrum is shown in (c). The average values of the diffusion coefficient for the three components, determined from well-resolved resonances, are indicated by the dashed lines. The values for quinine, geraniol, and camphene are 8.1, 11.6, and 15.6 $\times$ 10^{-6} cm^2 s^{-1}, respectively.

The region between 0.5 and 4.4 ppm is very crowded, and so the analysis of this region benefits significantly from the simplification obtained by decoupling. Expanded regions of both the conventional and decoupled spectra are shown in Fig. 26 (a) and (b).

DISCUSSION

The new method described in this paper is capable of yielding proton-decoupled proton spectra with absorption mode lineshapes and substantially correct integrals. The price that has to be paid for this decoupled spectrum is a considerable reduction in sensitivity when compared to a conventional proton spectrum, the need to record and process a complete two-dimensional spectrum, and certain difficulties associated with the need to suppress the cross peaks in the underlying two-dimensional spectrum. In addition, the presence of strong coupling leads to additional peaks in the decoupled spectrum – a feature that is not unique to our method.

There are a number of other ways of recording proton-decoupled proton spectra, and so it is useful at this point to compare these with the proposed new method.

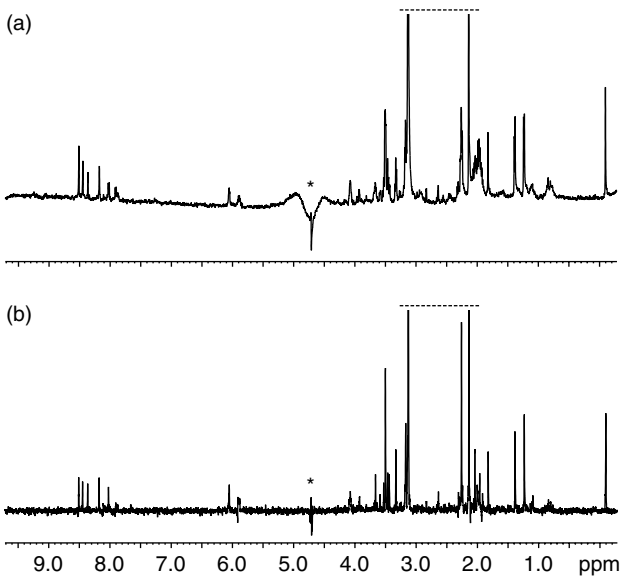

Figure 25. Broadband proton-decoupled proton spectrum of a sample of the cancer model cell extract in D_2O. The conventional proton spectrum, recorded with presaturation of the water signal, is shown in (a). The decoupled spectrum is shown in (b). In both spectra, the residual water signal can be seen on-resonance, and is labelled with a star.

Historically, the first method for recording such decoupled spectra was the use of a 45° projection of a two-dimensional *J*-spectrum.[20] The problem with this approach is that the two-dimensional spectrum has a phase-twist lineshape, the 45° projection of which is identically zero.[9] It is therefore necessary to project the absolute value spectrum, but unfortunately this gives an exceptionally broad lineshape, due to the dispersion mode contributions. These contributions can be eliminated by using strong weighting functions (in t_1 and t_2) to create symmetrical time-domain envelopes: this is the pseudo-echo method.[21] However, the drawback with such an approach is that the integrals of the peaks in the projection are very distorted, with broad peaks losing a great deal of intensity, to the point at which they may well disappear. In addition, even for sharp lines, there is a significant loss in intensity, as shaping the time-domain signals to a symmetric envelope eliminates that part of the signal where the intensity is greatest. Use of pseudo-echo weighting is certainly a practical way of obtaining a usable proton-decoupled proton spectrum, although it must be recognized that the intensity distortions are very significant.

Considerable effort has been put into finding alternative ways of processing two-dimensional *J*-spectra in such a way that the phase-twist lineshape is avoided. Such approaches typically involve replacing the phase-twists in the spectrum with a more favorable lineshape that has the same frequency and linewidth parameters, or nonlinear processing of the time-domain data.[22,23] Examples of the latter include linear prediction,[24] maximum entropy,[25] or filter diagonalization method (FDM).[26] At their best, these methods show promise, but they still suffer from distortions in the intensities of the projection – in particular, broad signals tend to be discriminated against quite strongly. These

DOI: 10.1002/mrc

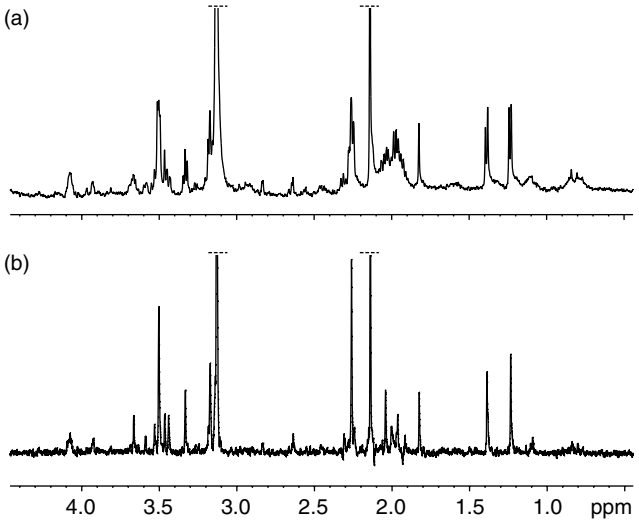

Figure 26. The crowded region of the spectra shown in Fig. 25. The conventional spectrum is shown in (a), and the decoupled spectrum is shown in (b).

nonlinear methods have failed to gain wide acceptance, probably reflecting more the difficulties of implementing 'non-standard' data processing than on any inherent defects with the approach.

There are three related methods that produce *J*-spectra in which the multiplets, rather than being aligned along the 45° diagonal, have structures with rotational symmetry patterns. For the first method, the *J*-spectrum is superimposed on its refection in the $\omega_1 = 0$ axis, creating a multiplet pattern in the form of a St. Andrew's cross.[27] For the other two techniques, the pulse sequence is modified to purge the anti-phase product operator terms present at the end of t_1. This is done by using either the inhomogeneity of the radiofrequency magnetic field orientated at the magic angle,[28,29] or a *z*-filter.[30] In all three cases, the resulting spectrum is processed with software which recognizes the symmetry patterns, thus constructing the decoupled spectrum.

Another approach to obtaining proton-decoupled proton spectra is to use the *constant time* method.[31,32] Here, a two-dimensional experiment is arranged so that scalar couplings evolve for a *fixed* time, whereas offsets evolve for the incrementable time t_1. As a result, the ω_1 dimension contains the required proton-decoupled proton spectrum, which can be in the absorption mode. The difficulty with this approach is that the intensities are modulated by the evolution of the scalar coupling during the fixed time, and are also weighted by relaxation during this time. Overall, therefore, in a system of any complexity the intensities are highly variable. A significant drawback of the constant time approach is that the decoupled spectrum appears in the ω_1 dimension, so obtaining high resolution can be time-consuming. It should be noted, however, that in biomolecular NMR the constant time approach is used to great effect, but the difference in such experiments is that the spin systems are well defined, and do not vary greatly from sample to sample, so that the constant time can be optimized in a straightforward way.

The method recently described by Zangger and Sterk[33] is of considerable interest. They use a selective refocusing pulse in the presence of a weak gradient that results, in effect, in all of the passive spins being flipped during a spin echo. As a result only the shift evolves during the echo, leading to a proton-decoupled proton spectrum. The required spectrum is not recorded in real time, but appears in the indirect dimension of a two-dimensional spectrum. However, it is possible to record the spectrum as an interferogram, sidestepping the need for recording or computing the complete two-dimensional matrix. The Zangger–Sterk method gives absorption mode lineshapes and substantially correct integrals. Like our method, there is a considerable reduction in sensitivity on account of the use of the selective pulse (we estimate that the two methods have comparable sensitivities). Recently, Nilsson and Morris have shown that the Zangger–Sterk method can be combined with diffusion weighting to give proton-decoupled DOSY spectra similar to those in Fig. 24.[34]

As has been pointed out, (Morris GA 2006, personal communication) our method and the Zangger–Sterk approach have an interesting similarity in that both achieve decoupling by manipulating the passive spins. The Zangger–Sterk method does this by using a selective pulse, whereas our method uses small flip angle pulses. However, the advantage of the Zangger–Sterk approach is that cross peaks are not generated. On the other hand, the Zangger–Sterk method requires one to choose the selectivity of the refocusing pulse which is a compromise between sensitivity and the ability to decouple nearby multiplets.

All of these methods fail in the presence of strong coupling, which usually results in the generation of extra unwanted signals ('artifacts') and perturbation of intensities. Such signals are genuine responses from the spin system – they are not really artifacts, but they are certainly unwanted. Recently, it has been shown that such signals can be removed from two-dimensional *J*-spectra, although at the expense of considerable time and effort.[13]

In conclusion, we believe that our method is a useful addition to the armory of NMR techniques for spectral simplification. It is straightforward to apply, does not require any special hardware, and it does not use any unusual data processing. We expect that the method will be particularly useful in the analysis of mixtures and in quantitative experiments such as DOSY.

Acknowledgements

AJP thanks the University of Cambridge for a Domestic Research Studentship, and RAEE thanks the EPSRC and Eli Lilly and Company for a studentship. We acknowledge Dr Michael Thrippleton (University of Glasgow) for many useful discussions. We are also grateful to Dr Andrew Phillips (Astra Zeneca, Macclesfield) for his support and interest in this project, and to Prof. Gareth Morris (University of Manchester) for a pre-print of Ref. 34 The loan of the cell extract sample from Dr Ulrich Günther (University of Birmingham) is gratefully acknowledged.

REFERENCES

1. Oschkinat H, Pastore A, Pfändler P, Bodenhausen G. *J. Magn. Reson.* 1986; **69**: 559.

2. Bodenhausen G, Freeman R, Morris GA, Turner DL. *J. Magn. Reson.* 1978; **31**: 75.
3. Kumar A. *J. Magn. Reson.* 1978; **30**: 227.
4. Wider G, Baumann R, Nagayama K, Ernst RR, Wüthrich K. *J. Magn. Reson.* 1981; **42**: 73.
5. Jeener J. *Ampere International Summer School*. Basko Polje: Yugoslavia, 1971.
6. Aue WP, Bartholdi E, Ernst RR. *J. Chem. Phys.* 1976; **64**: 2229.
7. Thrippleton MJ, Keeler J. *Angew. Chem., Int. Ed. Engl.* 2003; **42**: 3938.
8. Cano KE, Thrippleton MJ, Keeler J, Shaka AJ. *J. Magn. Reson.* 2004; **167**: 291.
9. Nagayama K, Bachmann P, Wüthrich K, Ernst RR. *J. Magn. Reson.* 1978; **31**: 133.
10. Ernst RR, Bodenhausen G, Wokaun A. *Principles of Nuclear Magnetic Resonance in One and Two Dimensions*. Clarendon Press: Oxford, 1987.
11. States DJ, Haberkorn RA, Ruben DJ. *J. Magn. Reson.* 1982; **48**: 286.
12. Macura S, Huang Y, Suter D, Ernst RR. *J. Magn. Reson.* 1981; **43**: 259.
13. Thrippleton MJ, Edden RAE, Keeler J. *J. Magn. Reson.* 2005; **174**: 97.
14. Sørensen OW, Griesinger C, Ernst RR. *J. Am. Chem. Soc.* 1985; **107**: 7778.
15. Smith MA, Hu H, Shaka AJ. *J. Magn. Reson.* 2001; **151**: 269.
16. Johnson CS. *Prog. NMR Spectrosc.* 1999; **34**: 203.
17. Stejskal EO, Tanner JE. *J. Chem. Phys.* 1965; **42**: 288.
18. Lounila J, Oikarinen K, Ingman P, Jokisaari J. *J. Magn. Reson., Ser. A* 1996; **118**: 50.
19. Lindon JC, Holmes E, Bollard ME, Stanley EG, Nicholson JK. *Biomarkers* 2004; **9**: 1.
20. Aue WP, Karhan J, Ernst RR. *J. Chem. Phys.* 1976; **64**: 4226.
21. Bax A, Freeman R, Morris GA. *J. Magn. Reson.* 1981; **43**: 333.
22. Shaka AJ, Keeler J, Freeman R. *J. Magn. Reson.* 1984; **56**: 294.
23. Woodley M, Freeman R. *J. Magn. Reson., Ser. A* 1994; **111**: 225.
24. Barkhuijsen H, de Beer R, Bovée WMMJ, van Ormondt D. *J. Magn. Reson.* 1985; **61**: 465.
25. Sibisi S. *Nature* 1983; **301**: 134.
26. Mandelshtam VA, Taylor HS, Shaka AJ. *J. Magn. Reson.* 1998; **133**: 304.
27. Woodley M, Freeman R. *J. Magn. Reson., Ser. A* 1994; **109**: 103.
28. Xu P, Wu X-L, Freeman R. *J. Magn. Reson.* 1991; **95**: 132.
29. Xu P, Wu X-L, Freeman R. *J. Am. Chem. Soc.* 1991; **113**: 3596.
30. Simova S, Sengstschmid H, Freeman R. *J. Magn. Reson.* 1997; **124**: 104.
31. Bax A, Mehlkopf AF, Smidt J. *J. Magn. Reson.* 1979; **35**: 167.
32. Bax A, Freeman R. *J. Magn. Reson.* 1981; **44**: 542.
33. Zangger K, Sterk H. *J. Magn. Reson.* 1997; **124**: 486.
34. Nilsson M, Morris GA. *Chem. Commun.* 2007; http://xlink.rsc.org?DOI=b617761a. DOI: 10.1039/b617761a.